Machine learning-based evaluation of dynamic thermal-tempering performance and thermal diversity for 107 Cambridge courtyards

Peng, Zhikai; Debnath, Ramit; Bardhan, Ronita; Steemers, Koen

DOI
10.1016/j.scs.2022.104275

Publication date
2023

Document Version
Final published version

Published in
Sustainable Cities and Society

Sustainable Cities and Society 88 (2023) 104275

Contents lists available at ScienceDirect

Sustainable Cities and Society

journal homepage: www.elsevier.com/locate/scs

Machine learning-based evaluation of dynamic thermal-tempering performance and thermal diversity for 107 Cambridge courtyards

Zhikai Peng [a,d,*], Ramit Debnath [b,c], Ronita Bardhan [a], Koen Steemers [a]

[a] Department of Architecture, University of Cambridge, 1-5 Scroope Terrace, Cambridge, CB2 1PX, United Kingdom
[b] Cambridge Zero, University of Cambridge, JJ Thomson Ave, Cambridge, CB3 0HE, United Kingdom
[c] Division of Humanities and Social Science, California Institute of Technology, 1200 E California Blvd, Pasadena, CA 91125, United States of America
[d] Faculty of Architecture and the Built Environment, Delft University of Technology, Julianalaan 134, Delft, 2628 BL, The Netherlands

ARTICLE INFO

Keywords:
Courtyard
Microclimate
Thermal tempering
Thermal diversity
Machine learning
Historical urban contexts

ABSTRACT

The dynamic thermal conditions profoundly impact on the quality of physical, cultural, and social experiences in courtyard spaces. This research aims to identify the microclimatic dissimilarities between courtyards in terms of tempering seasonal–diurnal thermal extremes and enriching ground-level thermal textures. The methodology included field measurements in summer-2021 and winter-2022 in Cambridge, UK; microclimatic simulations of 107 courtyards in ENVI-met and model validations; and machine learning-driven clustering using Super Organising Maps (SuperSOM). The results indicate that the diurnal thermal range of the spatial-UTCI mean in summer (DTR(M) < 24°C) is double that in winter (DTR(M) < 12°C); meanwhile the maximum spatial-UTCI deviation is three times as significant ($\delta > 3$°C at 7:00 BST versus $\delta > 1$°C at 12:00 GMT). SuperSOM analysis was performed using K-means and hierarchical agglomerative clustering to partition all courtyards into seven subclusters on its graph-lattice structure. Clusters Km_I, Hac_I, and Hac_IV feature a positive synergy between the thermal-tempering and thermal-enriching potentials. In contrast, the other four clusters exhibit conflicting scenarios during the day and night across the two seasons analysed. These data-driven outcomes enabled us to optimise spatial and landscape strategies for designing and retrofitting courtyard microclimates, contributing to the current discussions on climate-responsive and sensation-inclusive design in historical urban contexts.

Nomenclature

d_j	euclidean distance between neurons -
T_a	air temperature °C
T_d	dew point temperature °C
T_g	globe temperature °C
BMU	best matching unit -
BST	British summer time -
CA	courtyard area m^2
DTR	diurnal thermal range °C
GMT	greenwich mean time -
H/W	aspect ratio $m \cdot m^{-1}$
HAC	hierarchical agglomerative clustering -
HAR	horizontal aspect ratio $m \cdot m^{-1}$
LAT	long axial tilt Deg. (°)
$M(UTCI_{ij})$	mean of the surface dataset $UTCI_{ij}$ °C
MRT	mean radiant temperature °C
Pres	air pressure Pa
PWS	portable weather station -
RH	relative humidity %
RWS	roof weather station -
SI	shape index $m \cdot m^{-1}$
TE	thermal enriching -
TT	thermal tempering -
U	wind speed $m \cdot s^{-1}$
U_dir	wind direction Deg. (°)
UTCI	universal thermal climate index °C
VAR	vertical area ratio $m^2 \cdot m^{-2}$
VC_c_2d	tree coverage within the courtyard%
VC_c_3d	grass coverage within the courtyard%
$\delta(UTCI_{ij})$	standard deviation of the surface dataset $UTCI_{ij}$ °C

* Corresponding author.
E-mail address: zp254@cam.ac.uk (Z. Peng).

https://doi.org/10.1016/j.scs.2022.104275
Received 19 June 2022; Received in revised form 27 September 2022; Accepted 23 October 2022
Available online 26 October 2022

1. Introduction

Research into courtyard microclimate has a long history. The semi-enclosed, centralised outdoor spaces of courtyards, either in the form of gardens or patios, have been fundamental design elements in the vernacular townscape across many parts of the world. Not only do they contribute to attenuating the extreme heat, gusty wind, and noise, but they also collect the pleasurable sunlight and breeze to benefit users both indoors and outdoors. Courtyards have been frequently revisited as bioclimatic forms since the emergence of research interest in digital and modelling techniques to evaluate urban microclimate, daylight, and energy performance by changing buildings' geometric and landscape parameters based on real environmental observations. Martin and March (1972), in their '*Urban Space and Structures*' (Martin et al., 1972) investigated three distinct typologies of built forms: "pavilions," "streets, " and "courts", which were later reviewed and reassessed using the early computation techniques by Ratti et al. (2003). Their simulation demonstrated that the environmental performance (surface-to-volume ratio, shadow density and daylight distribution) of courtyard typology exceeds that of other built forms, such as pavilions, slabs, and terraces, especially in hot and arid climate. Raydan et al. (2004) indicated in their article titled '*Courtyards: A Bioclimatic Form*' that 'the key aspect in a search for an environmentally optimal urban configuration resides in the possibility and simplicity of carrying out parametric runs that test geometric modifications'. To date, most simulation studies have been validated through actual field measurements to demonstrate the significant contributions of courtyards to the climatic resilience of urban settlements. These expanding research efforts are aimed at providing more accurate predictions and employing advanced data analytical techniques to uncover the underlying science that governs the observations of dynamic thermal textures and human comfort in real-world built environments.

At district level, shadows substantial impact the microclimates within and between the courtyards. The mutual shadings cast by the buildings and trees can absorb both shortwave and longwave radiation, significantly offset the solar heat gains, and adjust the diurnal surface energy balance (SEB) between the roofs, walls and grounds. Besides the cooling and energy-saving benefits, urban shade can promote the use of outdoor space and nudge adaptive thermal behaviours of pedestrians in summer. However, shaded environments may not be deemed desirable at all times. Humidity-associated cold stress is a severe problem in excessively shaded outdoor space in cold and monsoon seasons. In this regard, optimising sun and wind exposure to counterbalance dynamic thermal needs is essential for improving seasonal and diurnal thermal comfort in public urban spaces.

This research was motivated by the synergistic and conflicting observations of courtyard microclimates between warm and cold seasons in the United Kingdom, which pose a challenge for selecting the optimal spatial and landscape strategies to improve intra-courtyard thermal conditions. Taking the sun path model in Cambridge as an example, even though a deep courtyard reduces solar heat gain and wind gusts, the humid conditions are not conducive to summer and winter thermal comfort (Fig. 1-a); a shallow and bare courtyard is more vulnerable to heatwaves, whereas the winter sun can still be beneficial in alleviating cold stress (Fig. 1-b); a small medium-depth courtyard can satisfy both sun and shade seekers in summer, while in high latitude countries, the ground remains fully shaded in winter (Fig. 1-c). Therefore, is a large medium-depth courtyard with adequate coverage of deciduous trees the one-size-fits-all solution that mitigates the heat and cold extremes and retains the most diverse thermal texture throughout the year (Fig. 1-d)?

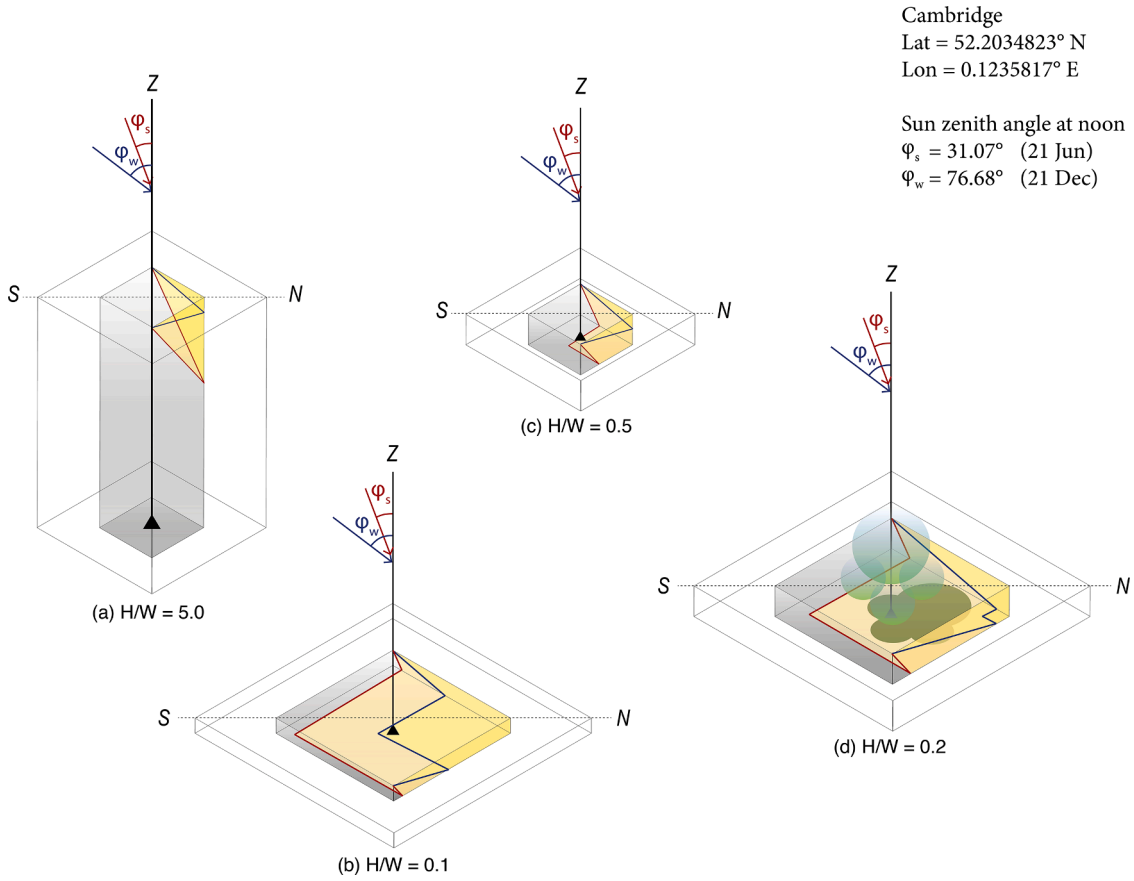

Fig. 1. Four courtyard axonometries based on the midday sun position in Cambridge, UK, with two shading lines cast in the summer solstice (dark red) and winter solstice (dark blue). (a) overshadowed-bare, (b) over-insolated-bare, (c) half-sun-half-shade-bare, (d) half-sun-half-shade-green.

The hypotheses based on these simple courtyard prototypes require further evidence from real measurements and accurate modelling in a range of large/small, deep/shallow, regular/distorted, and green/bare courtyards from real urban environments. Hence, three questions are proposed for 107 fully-enclosed courtyards in Cambridge, UK:

[Q1] How dissimilar are the outdoor thermal conditions within and between the courtyards of varying enclosure forms and landscape features?
[Q2] What drives the seasonal and diurnal dynamics of intra- and inter-courtyard thermal diversity?
[Q3] Are there optimal spatial and landscape strategies for retaining a non-extreme and diverse courtyard microclimate all year round?

The novelties of this study lie in the numeric microclimate modelling and longitudinal validations with these real courtyard geometries and landscapes, and the parametric techniques for analysing the Universal Thermal Climate Index (UTCI) maps. In addition, a machine-learning clustering approach – the Super (Self-)Organising Map (SuperSOM) – is applied to identify the dissimilarities in the UTCI maps of courtyards within the historical context in Cambridge. The scope of this paper is the outdoor thermal environments of courtyards, as the microclimate boundary of an enclosed geometry can be precisely defined and parameterised. Other types of urban thermal environments, such as streets and squares, have openings to the adjacent urban spaces that may increase the difficulties in defining the microclimate boundaries and ruling out the meteorological effects of the urban contexts.

2. Background

Extreme weather events have drawn worldwide attention to finding integrative thermal-adaptive solutions amidst global urban climate challenges. Outdoor thermal comfort modelling aims at more than the incorporation of these one-dimensional 'cold–warm' thermal indices because comfort does not necessarily result from a neutralised temperature but rather from diverse and dynamic sun and wind conditions. To date, two distinct thermal functions have been highlighted in courtyard comfort research across world climate zones: the thermal-tempering (TT) and thermal-enriching (TE) potentials.

2.1. Thermal-tempering (TT) potential

The TT potential indicates the degree of shielding abilities of courtyard against thermal extremes (heat/cold stress, wind gusts) from the external environment and regional climatic contexts, e.g., by comparing the air temperature within and outside the courtyard. Most of the study areas in the literature that highlight the TT potentials of the courtyards have been in hot-arid and tropical zones, where extreme heat events are more frequent than in the Global North. There is also a great emphasis on heat-related research in the European regions. For instance, deep and narrow patios with low sky exposure are common archetypes in Mediterranean regions to prevent solar excess and overheating issues in dense urban areas (Diz-Mellado et al., 2021). The diurnal thermal range (DTR) within deep courtyards can be 17 °C narrower than outside in southern Spain (Rivera-Gómez et al., 2019).

The tempering effect of courtyards also applies to mitigating cold stress induced by low air temperature and high wind speed. Unlike 'sun protectors' in warm regions, the semi-enclosed spaces are much shallower in colder climates. They serve as 'sun collectors' (Mänty & Pressman, 1988; Zamani et al., 2018). The designs of these courtyards are also aimed at reducing exposure to the external nuisance of wind and cold stress, such as in the Netherlands (Taleghani et al., 2014), the coastal regions of Sweden (Johansson & Yahia, 2020), and other oceanic-climate regions. However, few courtyard microclimates have been quantitatively investigated in more northerly cooler and humid European climates. This paper attempts to address this research gap by exploring the TT potentials of various courtyard forms in Cambridge, UK.

2.2. Thermal-enriching (TE) potential

The TE potential refers to the thermal diversity of the courtyard at two levels: (1) the variety of thermal conditions (e.g., sun-windward, shade-windward, sun-leeward and shade-leeward) within a single courtyard; (2) the microclimatic dissimilarities between different courtyards. Thermal delight (Heschong, 1979), arousal, and pleasure depend on the richness of the microclimate and local thermal texture (Steemers et al., 1997). Reynolds (2002) in *'Courtyard: Aesthetics, Social and Thermal Delight'* indicated that 'contrast is an essential ingredient of courtyard aesthetics, beginning with first transitions from the heat, noise, stench and glare of the street to the cool dark quiet of the zaguán[1]'. Steemers and Ramos (2009) and Nikoloupoulou (2001) indicated that outdoor comfort is 'determined by a complex combination of physical and psychological conditions'. Environmental diversity, namely the presence of sun, shade, wind, and stillness, is essential for meeting different individuals' perceived control and thermal needs (Nikolopoulou et al., 2001; Steemers & Ramos, 2009). Natural elements, such as dappled tree shade, small water bodies, and compositions of different pavement materials, also help to enrich the local thermal textures and promote restorativeness and biophilia in (semi-)open spaces (Beatley, 2011). Wada (2004) noted how the sun–shade ornamentation imposed by natural and geographical conditions might bring complexity and richness to a courtyard history (Edwards et al., 2006). An enriched thermal texture can meet a wider range of thermal preferences, reinforce thermal-psychological adaptability (Nikolopoulou, 2011), and promote thermal alliesthesial effects by contrasting hot and cold stimuli (Parkinson et al., 2012). Contrarily, isothermal places, such as huge empty squares without building enclosure, usually entail large sun and wind patches causing thermal boredom (Peng et al., 2022) and dissatisfaction even in mild seasons.

However, to the authors' knowledge, intra-courtyard thermal diversity has not been numerically assessed or been verified through longitudinal measurements. Chatzipoulka et al. (2020) defined a sun-wind diversity '*D*%' by using sun-path and wind-shadow-casting algorithms to determine the richness of sun–wind patches at the district level. The diurnal sun–wind diversity was shown to highly correlate with building density, coverage, and other urban spatial features; nonetheless, the static sun-path approach is limited in estimating hourly thermal diversity, let alone in capturing the thermal–physical exchange between air temperature, humidity, solar radiation, and air flow. Therefore, it is vital to introduce CFD-driven simulation tools and field measurement to understand the seasonality, diunality, and nocturnality of TE potentials in different courtyards, just as the TT potentials have been extensively studied.

2.3. AI and urban climate research

Artificial neural networks (ANNs) are considered some of the most efficient heuristic algorithms in dealing with high-dimensional data by parallel computation. Other statistical approaches may sacrifice optimality or accuracy due to the assumption of linearity in traditional regression models. The self-organising map (SOM) is an ANN algorithm for processing high-dimensional-low-sample-size (HDLS) datasets and detecting outliers. The SOM, also known as the Kohonen map (Kohonen, 1982), is one of the most widely applied unsupervised learning techniques in identifying spatial–temporal principles for environmental and ecological modelling results, such as synoptic climatology (Sheridan & Lee, 2011), air and water quality (Duan et al., 2022; Ejarque-Gonzalez & Butturini, 2014; Qu et al., 2021), land surface temperature (Hu & Weng,

[1] The passageway connecting the street and the courtyard

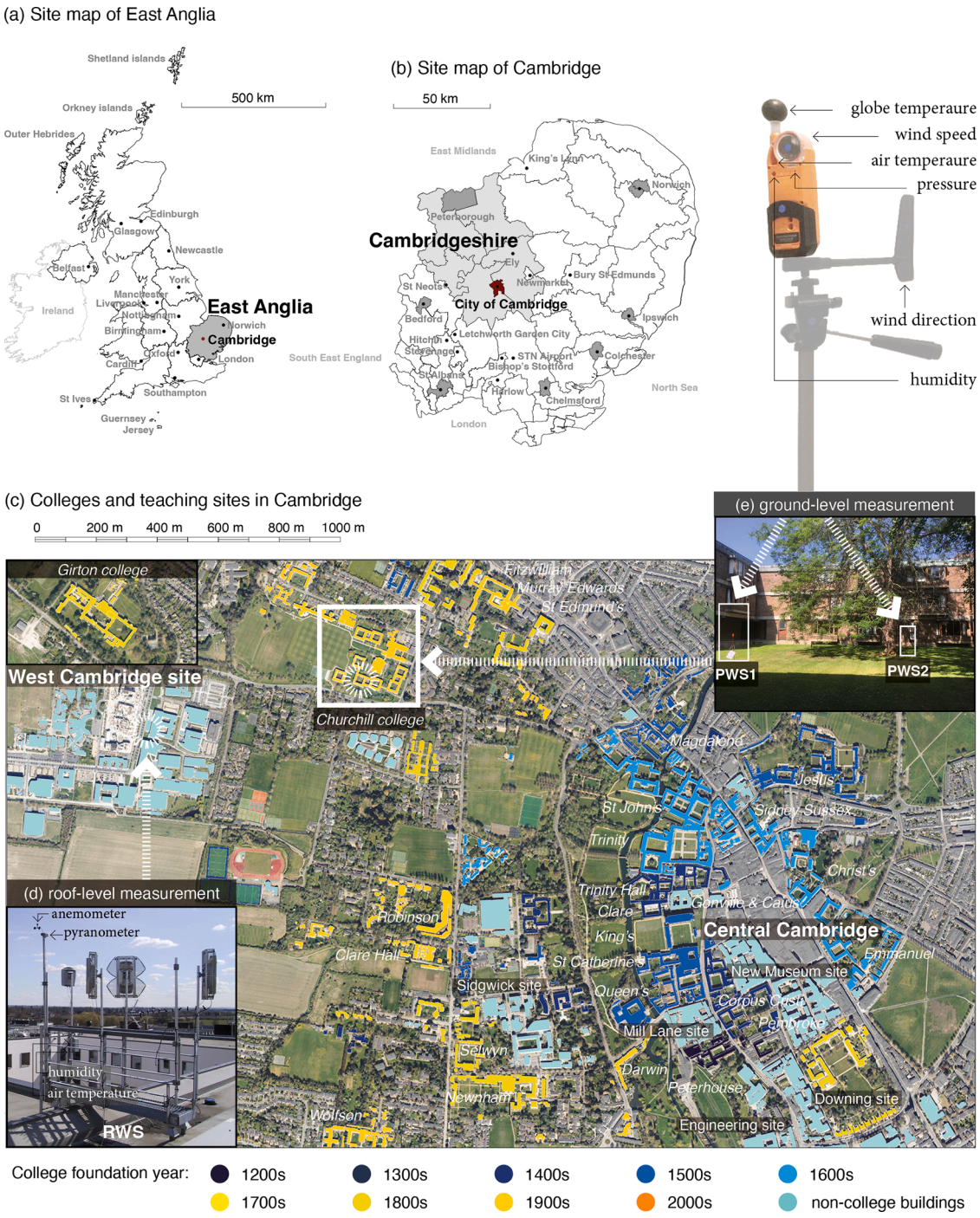

Fig. 2. Map showing: (a) & (b) locations of East Anglia and the city of Cambridge; (c) all courtyard locations and the foundation years of corresponding colleges/teaching sites in Cambridge; (d) the RWS location at Computer Laboratory in West Cam site; (e) the validation courtyard in Churchill College, with the two PWSs highlighted.

2009), biodiversity (Shanmuganathan et al., 2006), smart metering (Mcloughlin et al., 2015), and perceptions towards climate change (Sugg, 2021).

The exploration of urban climate research using the Kohonen map demonstrates its convenience of visual and comprehensive understanding of diurnal and seasonal climate behaviour. Compared with conventional linear regression methods, the application of the Kohonen map to courtyard microclimates is novel in the fields of outdoor thermal comfort and urban design. In this paper, we target the 'ENVI-met + Hybrid-SuperSOM' method to narrow the scope in a search for the optimal courtyard forms that can promote the synergy between TT and TE potentials throughout the year.

2.4. From climate-responsive to sensation-inclusive urban design

Climate-responsive urban design has grown in popularity in academic and design communities over the previous decades. Several courtyard studies introduced data-driven design tools to assess thermal discomfort under extreme scenarios, such as heat waves, gusty winds, and weather-related disasters and to support the decision-making process in sustainable urban design (Natanian & Auer, 2020).

However, non-extreme scenarios have been largely overlooked in the

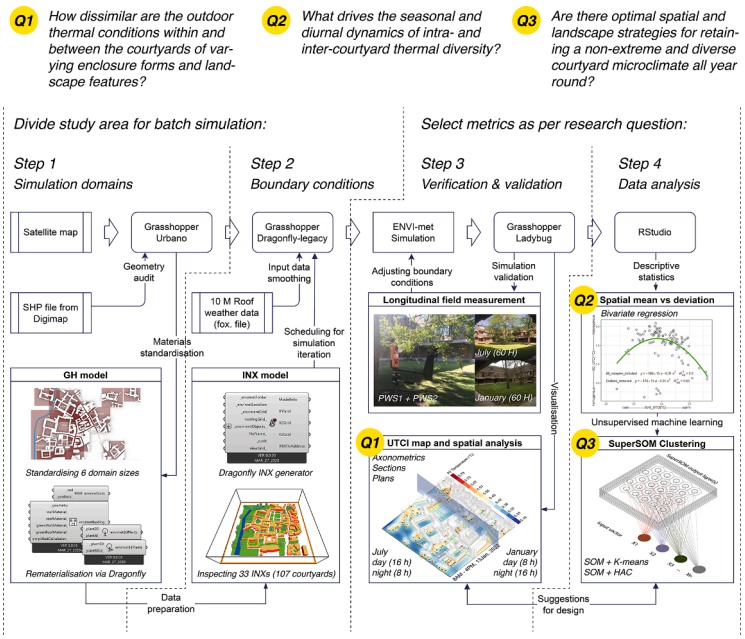

Fig. 3. The methodological framework in four steps.

modelling process due to the presumption that thermal neutrality (the absence of thermal extreme) would result in thermal satisfaction, proved by controlled experiments (Fanger, 1970). Such laboratory-led experimental conclusions may not necessarily hold true in (semi-)outdoor environments that are non-static (Liu et al., 2021; Peng et al., 2022). Outdoor thermal adaptation also depends on the diversity of thermal texture to ensure thermal equality (hot and cold preferences) and thermal pleasure (hot and cold contrast).

Future urban settlements are tasked with 'providing universal access to safe, inclusive, and accessible, green, and public spaces for all walks of life' (UN SDG 11.7) and 'the inclusion, resource efficiency, mitigation and adaptation to climate change, and resilience to disasters' (UN SDG 11.B) (Nations, 2015). Designing for human thermal comfort should include, rather than eradicate, those mild and ever-changing thermal stimuli that comprise the thermal texture of the built environment (Steemers et al., 1997). In light of this, this study introduces quantitative methods to evaluate thermal-tempering performance in tandem with thermal diversity to urge architects and urban designers to incorporate 'sensation-inclusive design' into their design practice.

3. Material and methods

3.1. Field measurements

The study area is Cambridge, United Kingdom (0.12°E, 52.20°N). The temperate oceanic climate in England falls into 'Cfb' in the Köppen climate classification (temperate, no dry seasons, warm summer). Due to the high latitude, Cambridge has greater diurnal and seasonal variations in sun positions than in southern Europe. This results in more than 15 h of daylight in the summer and fewer than 8 h in the winter. Hence, the courtyard microclimates' seasonality, diurnality, and nocturnality are prioritised for investigation. We screened all the courtyard urban fabrics in Cambridge and then pooled 107 fully-enclosed courtyards into the geo-database for batch ENVI-met simulation. Two separate field measurements were followed to validate the ENVI-met models in the summer (16–20 July 2021) and winter (10–14 January 2022), each lasting 120 h. This measurement schedule was adopted to use our limited measurement equipment effectively. One courtyard in Churchill College was chosen for measurement, because it satisfies all the following criteria: (1) close to the roof weather station (RWS) located at the Computer Laboratory in the West Cambridge site (Fig. 2-d), (2) explicit boundary conditions where the sun path is not obstructed by high towers/trees, (3) fully enclosed courtyard geometry, (4) trees and grasslands are both available, and (5) logistical concerns (accessibility, consent from the college, risks of instrument vandalism, etc). Two portable weather stations (PWSs) – Kestrel 5400 Heat Stress Trackers – were positioned within the Churchill courtyard, one on the south side and one beneath the tree on the north side (Fig. 2-e).

3.2. Analytical workflow

The 'ENVI-met simulation with field validation' and SuperSOM clustering techniques are used to investigate the thermal-tempering performance and thermal diversity amongst 107 courtyards in Cambridge. The methodological framework comprises four steps following three research questions (Fig. 3).

3.2.1. Simulation domains

The first step involved the setting of simulation domains (INX model). Then grasshopper (GH) was used to digitise and edit DigiMap geometry data. Next, on-site surveys of trees and plant species were conducted in all accessible courtyards to refine the ENVI-met model to correspond to the real situations. Additional tools, such as the aerial roaming in DigiMap and Google Earth 3D, were used to add missing landscape information in inaccessible courtyards.

The Dragonfly (DF) plug-in was used to rematerialise and convert the GH model to the INX model (grid size = 3 × 3 m, Z_0 = 2 m, telescoping factor = 18%) for the subsequent ENVI-met microclimate simulations (Chris Mackey et al., 2020; Natanian et al., 2019). ENVI-met software v4.4.6 was used, which features the Indexed View Sphere (IVS) algorithms to improve accuracy in modelling surface temperature and reflected radiation.

3.2.2. Boundary conditions

The second step defined the boundary conditions for the 33 INX models in GH. It then generated the forcing files (roof weather data) to be assigned to all INX models. The 10-metre roof data at the West Cambridge RWS were compared to two official RWSs located in Cambridge Acrefield and the Botanical Garden – both accessible via the MetOffice Integrated Data Archive System (MIDAS) (Office, 2012).

3.2.3. Verification and validation

The third step involved the validating the ENVI-met model against the measured data. By pre-testing one simulation domain, the trial modelling sessions ensures that the simulated conditions matched the real ones at the Churchill College site. The forcing files were readjusted to circumvent simulation errors caused by excessive z-axis telescoping (> 18%), inconsistent units (K versus °C, knot versus $m{\cdot}s^{-1}$), instability during initialisation (ENVI-met cannot decrease the relaxation factor when the boundary wind inlet $U < 0.5\ m{\cdot}s^{-1}$ or abrupt/frequent changes in U_dir > 135° every 30 mins), and temporal dislocation between the ENVI-met default radiation data and the roof temperature data (due to the summer daylight saving adopted by the RWS). Following numerous rounds of error checking, the batch simulations of 33 INX models were executed iteratively in ENVI-core and took around 40 days to complete.

3.2.4. Data analysis

The final step included spatial analysis, descriptive statistics, and machine learning-based clustering. The ENVI-met results were reprocessed in GH to compute the hourly spatial mean and spatial deviations (for 48 h) of all 107 courtyards based on their universal thermal climate index (UTCI) maps. The simulation data from the first day were removed since they may be less equilibrated than the data from the second day (2^{nd} 24-hour) (Jacobs et al., 2020; López-Cabeza et al., 2018). Descriptive statistics were run to identify the diurnal principles of the TT and TE potentials in the two seasons. Finally, 96 microclimatic variables were tabulated into a new dataset for the SuperSOM clustering, of which the results were compared with 7 morphological variables of each courtyard for further analysis. The following three sections address data, metrics, and clustering techniques at greater length.

3.3. Data

3.3.1. Validation data

The raw data from the two PWSs are sampled at five-second intervals and contain the air pressure (*pres*), globe temperature (T_g), T_a, *RH*, *U*, and *U_dir*. After averaging the raw measurement data into hourly intervals, most of them can be used directly to validate the simulation results, except for T_g, which requires pre-conversion (Standard, 1998) to mean radiant temperature (MRT) (Eq. (1)).

$$MRT = \left[\left(T_g + 273.15\right)^4 + \frac{1.1 \times 10^8 \times U^{0.6}}{\varepsilon d^{0.4}} \left(T_g - T_a\right) \right]^{0.25} - 273.15 \tag{1}$$

where the globe emissivity $\varepsilon = 0.95$, and diameter $d = 25.4$mm.

3.3.2. Thermal indices

The compound thermal indices can nomographically determine the combined effects of temperature, humidity, radiation, and wind in the ENVI-met outputs as one of the most extensively studied biometeorological metrics for humans. UTCI can estimate the intensity of thermal stress in a non-uniform and transient outdoor environment compounded by dynamic sun and wind conditions (Park et al., 2014). UTCI uses the same unit as T_a and can be calculated using the Ladybug (LB) plug- in GH (Perini et al., 2017) (Eq. (2)). The inputs for the UTCI calculation, including *RH*, *MRT*, & *U*, are devoid of subjective characteristics such as age, metabolic rate, and amount of clothing (Jendritzky et al., 2012).

$$UTCI = f(T_a,\ RH,\ MRT,\ U_{10m}) \tag{2}$$

where U must be transformed from 1.5 m to 10 m wind using a logarithmic method that approximates the vertical wind profile (Havenith et al., 2012) (Eq. (3)).

$$U_{10m} = U_{1.5m} \times log(Z/Z_0) \times log(Z_R/Z_0)^{-1} \tag{3}$$

Where $Z = 1.5$ m denotes the midpoint on a grid height (3m), $Z_R = 10$ m, and $Z_0 = 0.01$ m.

3.4. Metrics

3.4.1. Validation metrics

Root mean square error (*RMSE*) is an accuracy metric (Eq. (4)) used to validate the ENVI-met results against the measurement data. The ENVI-met results are sampled at four grids (36 m^2) in GH that correspond to the actual measurement locations of PWS1 and PWS2 in the Churchill College courtyard. The validation procedure entails comparing the *RMSE*s for the original values, T_a, *RH*, MRT, and *U*, at each location and the deviation values, *delta*(T_a), *delta*(*RH*), *delta*(*MRT*), *delta*(*U*), between the two locations – one in the sun and the other in the shade. The simulation accuracy results were then benchmarked against the relevant literature (Forouzandeh, 2021; López-Cabeza et al., 2018; Salata et al., 2016).

$$RMSE(X_t,\ \widehat{X}_t) = \sqrt{\frac{1}{T}\sum_{t=1}^{T}(X_t - \widehat{X}_t)^2} \tag{4}$$

where X_t is the measurement data and $\widehat{X_t}$ is the simulation data; T is the length of the time series (here two window periods $t \le 24$ and $25 \le t \le 48$ are compared to examine the accuracy improvement during the 2nd 24-hour simulation).

3.4.2. Spatial-UTCI mean

The TT potential can be quantified by benchmarking each courtyard's spatial mean of UTCI against the global mean of UTCI of all simulation domains. The spatial mean metric is applied to the grids encircled by the inner boundary of each courtyard (Eq. (5)). Each courtyard outputs a unique time-series of spatial mean for further analysis of morphological effects through hybrid-clustering methods.

$$M\left(UTCI_{ij}\right) = \frac{1}{N}\sum_{i=1}^{N} UTCI_i \tag{5}$$

where $UTCI_{ij}$ is the gridded map for analysis, ranging from grid *i* to *j*; $N = j$ is the size of the gridded dataset; $UTCI_i$ is the data attributed to grid *i*.

3.4.3. Spatial-UTCI deviation

The TE potential can be quantified by benchmarking the spatial deviations of UTCI between different courtyards. The spatial deviation metric Aune-Lundberg & Strand, 2014) indicates the degree to which the thermal conditions are comparatively enriched in a courtyard (Eqs. (6), ((7)). The morphological effects of enclosure geometry and tree configuration on spatial-UTCI deviation were found greater than on spatial-UTCI mean, based on the multiple regression method in our previous work (Peng et al., 2022).

$$\delta^2\left(UTCI_{ij}\right) = \frac{1}{N}\sum_{i=1}^{N}\left[UTCI_i - M\left(UTCI_{ij}\right)\right]^2 \tag{6}$$

$$\delta\left(UTCI_{ij}\right) = \sqrt{\delta^2\left(UTCI_{ij}\right)} \tag{7}$$

3.4.4. Morphometrics

Seven morphometrics in this study have been referenced from relevant literature to quantify the courtyard building and landscape features. They are courtyard area (CA) Rojas-Fernández et al., 2017; Yaşa & Ok, 2014), vertical area ratio (VAR) (Bardhan et al., 2018; Mehrotra et al., 2020; Ratti et al., 2005), shape index (SI) (Bogaert et al., 2000; Shirowzhan et al., 2018), horizontal aspect ratio (HAR) (Manioğlu & Oral, 2015; Soflaei et al., 2017), long axial tilt (LAT) (Berkovic et al., 2012; Moonen et al., 2011; Rodríguez-Algeciras et al., 2018; Taleghani et al., 2014), 2D vegetation (VC_c_2d) and 3D vegetation within the courtyard (VC_c_3d) (Darvish et al., 2021; Del Rio et al., 2019) (Eqs. (8)–((14)). All calculations were carried out in GH using Boolean methods.

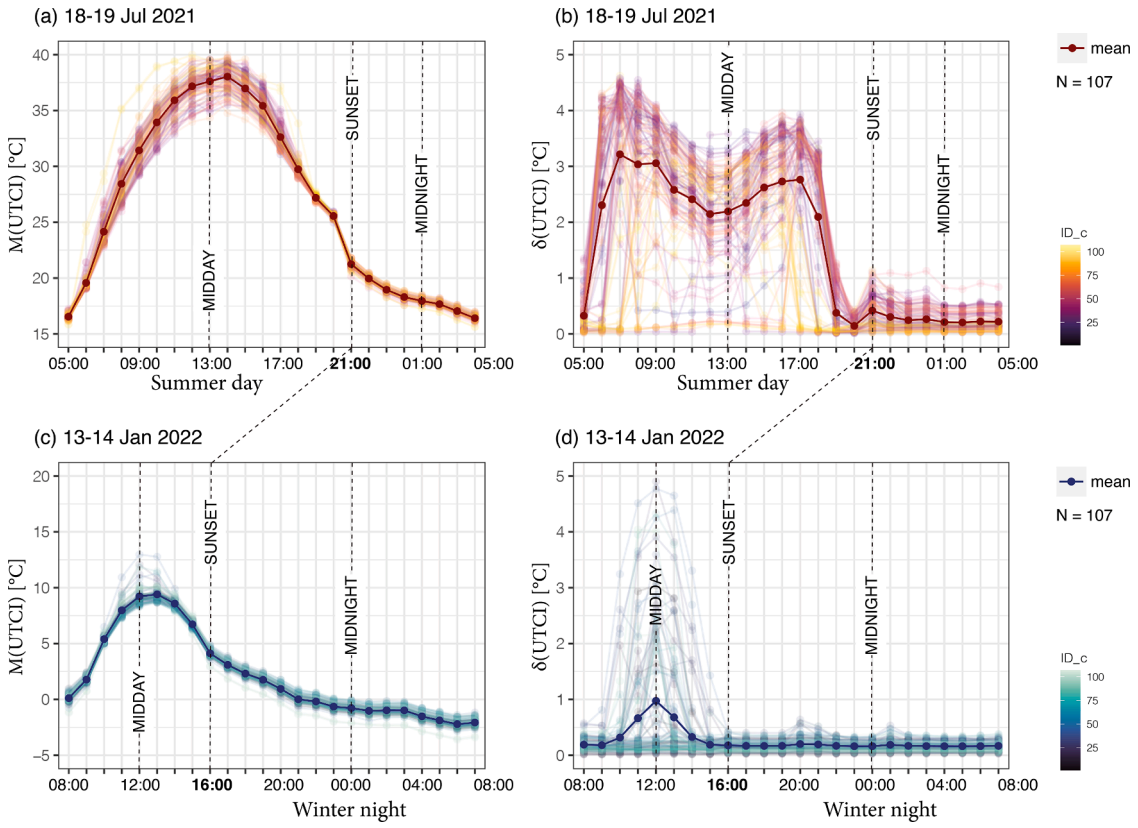

Fig. 4. The second 24-hour simulation results of 107 Cambridge courtyards were retained for the spatial analysis of UTCI maps at 1.5 m: (a) and (c) for spatial-UTCI mean, (b) and (d) for spatial-UTCI deviation. ID_c denotes the colour gradient lines sorted by courtyard sample ID.

$$CA(P) = \int_{i=1}^{N} \alpha_{ij} d(P) \tag{8}$$

where α_{ij} denotes each GH unit within the enclosed polyline that defines the inner courtyard perimeter P.

$$VAR(P) = VA(P)/CA(P) \tag{9}$$

where $VA(P)$ is the vertical area of the courtyard's inner facades (including the setbacks, arcades, and towers).

$$SI(P) = (P/4) \times CA(P)^{-0.5} \tag{10}$$

$$HAR = L/W \tag{11}$$

where L is the length of the long axis of the courtyard and W the short axis.

$$LAT = \theta(L) \tag{12}$$

where θ is the degree clockwise from north (0°) for the long axis.

$$VC\_c\_2d(P) = VA\_2d(P)/CA(P) \tag{13}$$

$$VC\_c\_3d(P) = VA\_3d(P)/CA(P) \tag{14}$$

where $VA\_2d(P)$ denotes the ground area covered by the grass and $VA\_3d(P)$ by the trees within the courtyard.

3.5. Machine learning-based clustering: supersom approach

The SOM is a competitive learning algorithm based on linear arrays of nodes on a 2D lattice framework Fig. 3, step 4). During each iteration of the learning process, all nodes maximally respond to a given input vector chosen to be the winning neuron (also called the best matching unit, 'BMU') by reducing their Euclidean distances d_j, between the weights w_{ij} and the input vector x_i (Eqs. (15) & (16), referenced from Chon et al., 1996 (Chon et al., 1996)). Other non-Euclidean distance functions, such as Manhattan distance (based on absolute distance, as opposed to squared error), were not used in this work due to the limited customisation options in the kohonen::som(R) package. At same time, they are worthy of further investigations if variables with heterogeneous properties, such as daylight, acoustics, air quality, etc., are mixed as input vectors for the SOM learning process.

$$d_j(t) = \sum_{i=0}^{N-1} \left[x_i - w_{ij}(t)\right]^2 \tag{15}$$

$$w_{ij}(t+1) = w_{ij}(t) + \eta(t)\left[x_i - w_{ij}(t)\right] Z_j \tag{16}$$

where i denotes the input layer and j the output layer; $w_{ij}(t)$ is set to small random values when $t = 0$; x_i is the input vector (here x_i are the hourly spatial mean and spatial deviation of the UTCI map of each courtyard); Z_j is assigned 1 for BMU and the neighbouring neurons, and 0 for the remaining neurons; $\eta(t)$ denotes the fractional increments of corrections and decreases by small values at each iteration t until the SOM obtains convergence. After reaching equilibrium, all samples are projected on the output layer (visualised in a 2D hexagonal map). Their locations on the SOM map and the neighbour distance (the cells shaded in gradient colour) indicate the closeness/dissimilarity amongst sub-communities.

The SOM reveals the topological relationships (how dissimilar are the microclimates) between the 107 courtyards on a 2D hexagonal map created by incrementally learning the 96-hour spatial mean and spatial deviation UTCI maps. The number of neurons ($M = 6 \times 9 = 54$) of the SOM can be estimated from the sample size ($N = 107$) (Tian et al., 2014) (Eq. (17)):

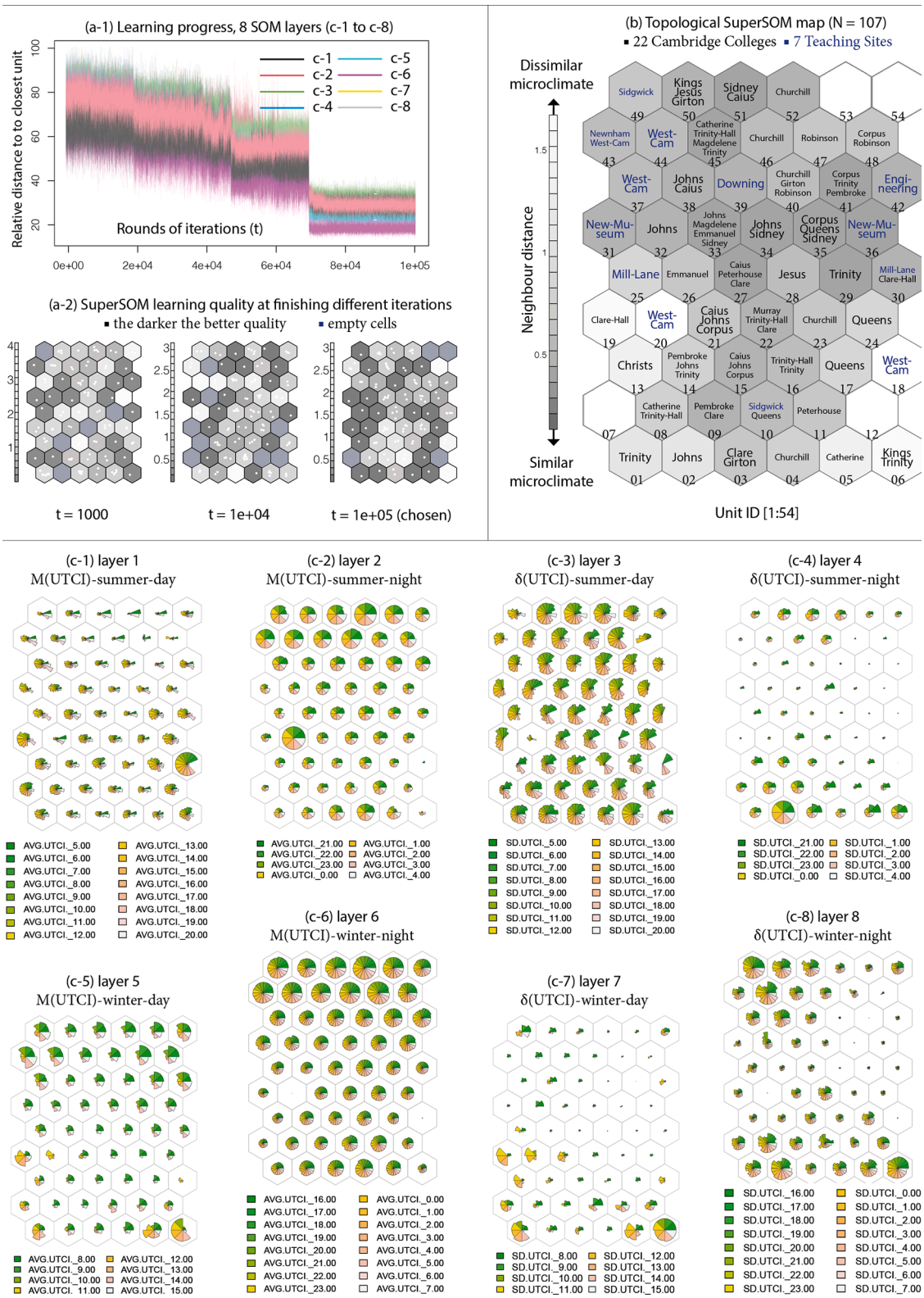

Fig. 5. The learning qualities (a-2) were compared at different iterations (a-1). The learning result of the final SuperSOM map provides (b) the topological structure of all 107 courtyards affiliated with 22 colleges and 7 teaching sites. The learning progress is based on incrementally changing the weights of 96 input vectors. The final weights are shown in the code plots. They are stratified into 8 layers, 4 in summer (c-1, c-2, c-3, c-4) and 4 in winter (c-5, c-6, c-7, c-8).

$$M \approx 5\sqrt{N} \tag{17}$$

Additional partitioning of the data is required, as 54 is still considered a large mesh of neurons for identifying multidimensional features (Costa & Netto, 1999). K-means and hierarchical agglomerative clustering (HAC) methods are used to further classify the 54 neurons based on their Euclidean distance d_j (Brentan et al., 2018). Discriminant analysis follows, using the Kruskal–Wallis one-way analysis of variance (K–W test) and Mann–Whitney U test to examine the cluster validity and

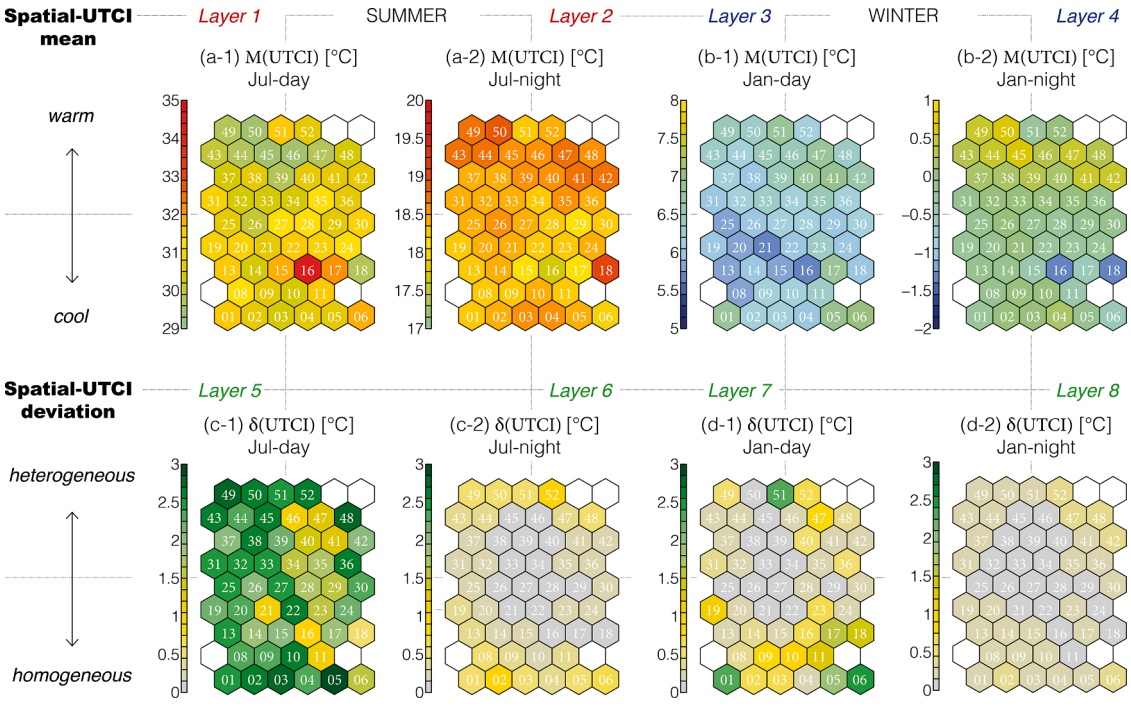

Fig. 6. The TT effect in summer (a-1–2) and winter (b-1–2), and the TE effect in summer (c-1–2) and winter (d-1–2). The neuron ID has been marked within each hexon [1:54].

to determine whether synergistic or conflicting TT and TE potentials are significant in each of the K-means and HAC clusters.

The learning progress and learning quality were examined using 'supersom' function in RStudio (package name 'kohonen', version 3.0) (Wehrens & Buydens, 2007). The supersom function maintains the same learning results as the 'som' function, while stratifying the 96 vectors into $2^3 = 8$ layers (with three subsets by $M(UTCI)$ & $\delta(UTCI)$, day & night, summer & winter) and visualises the vector weights in a lattice code plot. The input vectors of $M(UTCI)$ and $\delta(UTCI)$ were normalised ($0 < x_i < 1$), and the output SuperSOM maps were plotted in the original units [°C] for better readability. The code for reproducibility of the research is available at the following GitHub link (https://github.com/ZP254/SuperSOM-code-for-mapping-microclimate-dissimilarity.git).

4. Results

4.1. Validation and verification

After several debugging and testing rounds, the ENVI-met results show good agreement with the two PWSs data points in the Churchill courtyard. The differences are small between the measured and simulated T_a and RH ($RMSE = 1.7$ °C and 9%), and likewise, no significant simulation inaccuracies are found in the spatial-deviation measurements $delta(T_a)$ and $delta(RH)$ ($RMSE = 2$ °C and 6%) between PWS1 and PWS2 (Appendix B, Fig. B.1). The validations of the radiative and convective environments exhibit slightly higher inaccuracy: the *RMSEs* of *MRT* and *U* are controlled within 8 °C and 0.3 $m{\cdot}s^{-1}$, whereas those of $delta(MRT)$ and $delta(U)$ are less than 12 °C and 0.14 $m{\cdot}m^{-1}$ (Appendix B, Fig. B.2).

4.2. Dynamic thermal simulation of the courtyards

The batch ENVI-met simulation results show distinct diurnal behaviours between $M(UTCI)$ and $\delta(UTCI)$ for 107 courtyards in the two seasons (Fig. 4). In summer, the $M(UTCI)$ curve demonstrates a single peak at 14 BST (38 °C), which is similar to the air temperature curve. The $\delta(UTCI)$ curve fluctuates significantly more due to building-geometry and landscape effects, showing two peaks at 7:00 BST (3.2 °C) and 17:00 BST (2.9 °C). Both $\boldsymbol{M(UTCI)}$ and $\boldsymbol{\delta(UTCI)}$ curves peak only once, at 13:00 GMT (10 °C) and 12:00 GMT (1 °C) respectively, in winter. The diurnal range of $\boldsymbol{M(UTCI)}$ in summer (< 24 °C) is twice that in winter (< 12 °C), while the diurnal range of $\boldsymbol{\delta(UTCI)}$ in summer (< 3 °C) is three times than that in winter (< 1 °C).

4.3. Learning progress

The SuperSOM was used to learn the UTCI maps of the 107 courtyards. The 2nd 24-hour window period of the $\boldsymbol{M(UTCI)}$ and $\boldsymbol{\delta(UTCI)}$ simulation data is preserved as learning material for the SuperSOM algorithms. The final SOM topological map (TT and TE dissimilarity map) is visualised on a 2D lattice network.

4.3.1. Dissimilarity between courtyards' microclimates [Q1]

As shown in Fig. 5, the learning costs vary between 10 s and 3 min (macOS 12.1, 2.4 GHz Quad-Core Intel Core i5) depending on the iteration steps ($t = 1000$, 1e+04, 1e+05) predefined in R v4.2.1, where $t =$ 1e+05 yields the best learning quality (Fig. 5a-2). Neurons 07, 12, 53, and 54 are empty, whereas the rest have an average of two courtyard samples per neuron (Fig. 5b). The sample distribution and neighbour distances reflect the outliers/dissimilarities/nuances in $\boldsymbol{M(UTCI)}$ and $\boldsymbol{\delta(UTCI)}$ curves in the 107 courtyards. The weights of the 96 vectors are compared using 'code plots' to stratify and deduce the learning progress in eight layers. Each layer reflects one seasonal-diurnal pattern in the spatial-UTCI mean and deviation. The layer $\boldsymbol{\delta(UTCI)}$-summer-day (Fig. 5c-3) shares the largest portion of active neurons, followed by $\boldsymbol{M(UTCI)}$-winter-night (c-6) and $\boldsymbol{M(UTCI)}$-summer-night (Fig. 5c-2).

4.3.2. Seasonal and diurnal variability [Q2]

The results of the gradient UTCI maps (Fig. 6) are consistent with the d_j reduction mechanisms in SuperSOM where the neighbouring neurons are activated by the winning neuron (BMU). Each neuron has been shaded with a gradient of colours according to the original $\boldsymbol{M(UTCI)}$ and $\boldsymbol{\delta(UTCI)}$ data in Fig. 6. Courtyards with similar TT and TE potentials are classified closer in distance. For example, the neurons [01:10] and

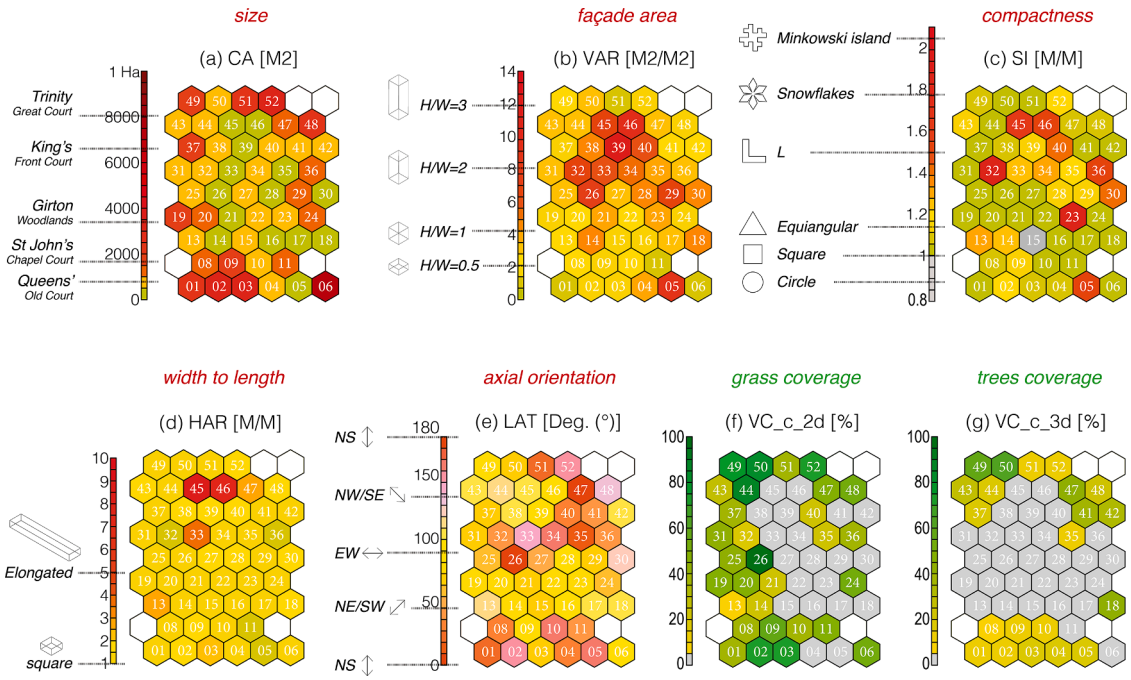

Fig. 7. The seven morphometrics maps are based on five building parameters (a-e) and two landscape parameters (f, g). The neuron ID has been marked within each hexon [1:54].

Table 1
Clustering validities between K-means and HAC methods (significance *P < .05, **P < .01, ***P < .001, **** < 0.0001).

Number of clusters (K)	K-means clustering ($N = 107$)							
	P-value for K-W test using $\boldsymbol{M}(\boldsymbol{UTCI})$ at 1.5M				P-value for K-W test using $\boldsymbol{\delta}(\boldsymbol{UTCI})$ at 1.5M			
	Jul-day	Jul-night	Jan-day	Jan-night	Jul-day	Jul-night	Jan-day	Jan-night
2	*.472*	*.069*	**	*.652*	*	*.246*	*.897*	*.084*
3 (chosen)	*	*	**	*	****	***	*.068*	**
4	*.881*	*.723*	**	*.571*	*.051*	*.157*	*	*
5	*.050*	*.165*	*	*.155*	***	*.065*	*	*.180*
6	*.190*	*.201*	**	*.439*	***	*.176*	*.554*	*.230*
7	**	**	**	*	**	*.321*	*.549*	*.191*
8	**	**	***	**	*	*.373*	*.543*	*
Number of clusters (K)	HAC clustering ($N = 107$)							
	P-value for K-W test using $\boldsymbol{M}(\boldsymbol{UTCI})$ at 1.5M				P-value for K-W test using $\boldsymbol{\delta}(\boldsymbol{UTCI})$ at 1.5M			
	Jul-day	Jul-night	Jan-day	Jan-night	Jul-day	Jul-night	Jan-day	Jan-night
2	*.342*	*.071*	*	*.568*	*	*	**	**
3	*.413*	*.146*	*	*.769*	*	*	*	*
4 (chosen)	**	*	*.090*	*.111*	**	*	*	*
5	*	*	*	*	**	*	*.074*	*.056*
6	*	*.059*	**	*	**	*	*.082*	**
7	*	*.073*	**	*.057*	*	*.052*	**	**
8	*	*	**	*	*	*	**	**

[43:52] feature more neutral $\boldsymbol{M}(\boldsymbol{UTCI})$ and higher $\boldsymbol{\delta}(\boldsymbol{UTCI})$ (cool-summer-warm-winter). Also, some outliers have been detected, such as neurons 16 and 18 (warm-summer-cool-winter), neuron 21(homogenous-summer-homogenous-winter) and neurons 01, 06, 51 (heterogenous-summer-heterogenous-winter).

4.3.3. *Building geometry and landscape [Q3]*

The seven morphometric maps (Fig. 7) demonstrate strong ties with the previous TT and TE dissimilarity maps. Likewise, we observe one or two outliers on the morphometric maps, e.g., small courtyards are often activated by the neurons in the centre (Fig. 7a). Each neuron is associated with specific courtyard morphometric data. Deep courtyards with high VAR (façade ratio) (Fig. 7b) are attracted by the neurons [32:34], [38:40], and [45:46], and so are those elongated and irregular courtyards quantified by SI (Fig. 7c) and HAR (Fig. 7d) metrics. Fewer outliers were found in the LAT (the orientation of the central axis) map (Fig. 7e) than in the other morphometric maps. Regarding the landscape maps (Fig. 7f, g), the neurons [1:10] and [43:52] are assigned with higher coverages of trees and grasslands. At same time, their positions are marginalised on the maps.

Note that the SuperSOM learning algorithm does not incorporate morphometrics and hence does not represent the geometric topology but rather the TT and TE dissimilarity. This is because (1) the research questions focus on the dissimilarity of microclimate rather than the dissimilarity of courtyard geometries; (2) some morphometrics were proved either positively or negatively correlated with the UTCI data and thus could confound the SuperSOM results (similar to multicollinearity issues) (Peng et al., 2022).

Table 2
Pair-wise discriminant analysis between K-means clusters ($K = 3$) and HAC clusters ($K = 4$). A significant TT effect in a cluster is benchmarked by the mean of all simulation domains ($< \boldsymbol{M_d}$ in summer and $\geq \boldsymbol{M_d}$ in winter); a significant TE effect is benchmarked by the mean of all courtyards ($> \boldsymbol{M_c}$) (significance *$P < .05$, **$P < .01$, ***$P < .001$, **** < 0.0001).

	N	$\boldsymbol{M}(\boldsymbol{UTCI})$ [°C] at 1.5M				$\boldsymbol{\delta}(\boldsymbol{UTCI})$ [°C] at 1.5M			
		Jul-day	Jul-night	Jan-day	Jan-night	Jul-day	Jul-night	Jan-day	Jan-night
Mean of all courtyards ($\boldsymbol{M_c}$)	107	30.7	18.4	6.1	0.0	2.15	0.26	0.44	0.17
Mean of all simulation domains ($\boldsymbol{M_d}$)	33	31.3	17.2	7.5	−1.0	2.71	1.06	2.50	1.20
Difference between K-means clusters ($K = 3$)									
Km_I	24	−0.9	+1.4	−1.3	+1.2	+0.29	+0.05	−0.07	+0.02
Km_II	54	−0.7	+1.2	−1.4	+1.0	+0.06	+0.02	+0.04	+0.01
Km_III	29	−0.3	+1.1	−1.2	+0.9	−0.36	−0.08	−0.01	−0.04
Mann-Whitney U test between K-means clusters	N	P-value for $\boldsymbol{M}(\boldsymbol{UTCI})$				P-value for $\boldsymbol{\delta}(\boldsymbol{UTCI})$			
Km_I-II	78	*.052*	*.088*	*	*	*	*.433*	*.349*	*.953*
Km_I-III	53	*	**	*.307*	*	****	**	*.110*	**
Km_II-III	83	*.258*	*.073*	**	*.738*	**	***	*	**
	N	$\boldsymbol{M}(\boldsymbol{UTCI})$ [°C] at 1.5M				$\boldsymbol{\delta}(\boldsymbol{UTCI})$ [°C] at 1.5M			
Difference between HAC clusters ($K = 4$)									
Hac_I	25	−0.8	+1.3	−1.3	+1.0	+0.16	−0.01	+0.09	+0.01
Hac_II	21	0.0	+1.1	−1.3	+0.8	−0.41	−0.06	+0.07	−0.02
Hac_III	46	−0.7	+1.2	−1.4	+1.0	+0.07	+0.04	−0.01	+0.02
Hac_IV	15	−1.0	+1.3	−1.3	+1.2	+0.07	0.00	−0.23	−0.04
Mann-Whitney U test between HAC clusters	N	P-value for $\boldsymbol{M}(\boldsymbol{UTCI})$				P-value for $\boldsymbol{\delta}(\boldsymbol{UTCI})$			
Hac_I-II	46	**	**	*.501*	*.080*	***	*	*	*
Hac_I-III	71	*.273*	*.392*	*.096*	*.620*	*.238*	*.242*	*.554*	*.476*
Hac_I-IV	40	*.211*	*.847*	*.406*	*.332*	*.600*	*.847*	*	*.173*
Hac_II-III	67	*	*	*.071*	*.104*	**	**	*.163*	*
Hac_II-IV	36	**	*	*.485*	*	*	*	*.800*	*.924*
Hac_III-IV	61	*.072*	*.567*	*.061*	*.191*	*.601*	*.470*	*	*

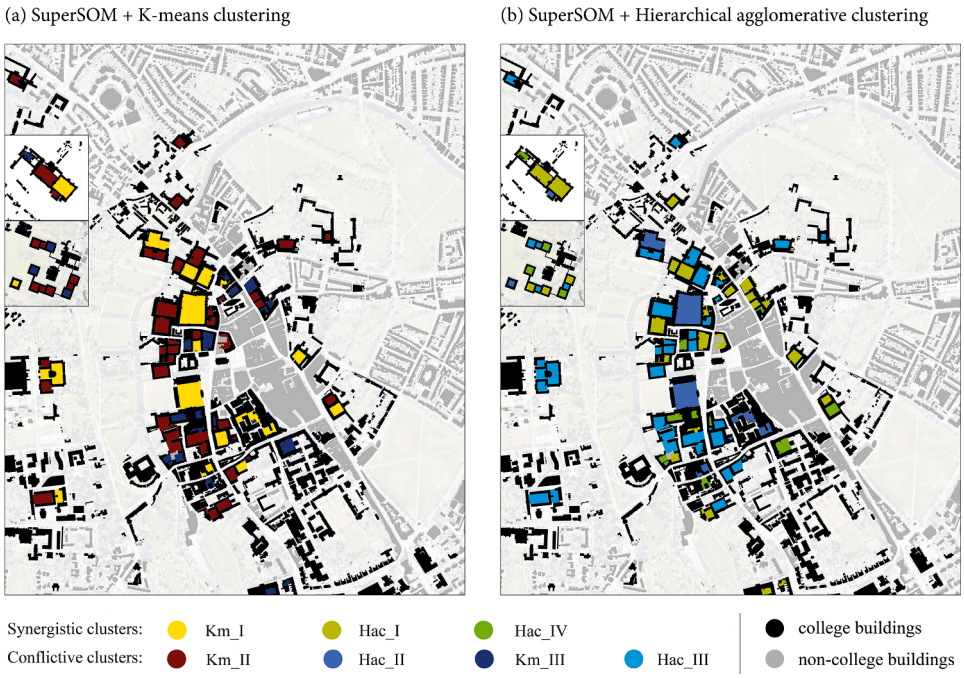

Fig. 8. Two maps of Cambridge showing microclimate dissimilarity amongst 107 courtyards based on hybrid SuperSOM clustering using K-means (a) and HAC (b) algorithms, respectively.

4.3.4. *Hybrid SuperSOM*

The qualitative manner of neuron-by-neuron interpretation might overlook the inter-hierarchical border on the 2D lattice map. According to the between-neuron $\boldsymbol{d_j}$ from the previous learning progress, two hybrid approaches – SuperSOM+*K*-means (top-down) and SuperSOM+HAC (bottom-up) – were compared in terms of their clustering validity over the SOM neurons of similar microclimate. To find the optimal K partitions, we adhere to the rule of thumb that too few clusters result in biases, while too many clusters complicate the interpretation of $\boldsymbol{M}(\boldsymbol{UTCI})$ and $\boldsymbol{\delta}(\boldsymbol{UTCI})$. The initial choice of the optimal K

Table 3
Summary of courtyard microclimatic effects based on this study and other literature review in temperate climates ('sig.' for significant; 'insig.' for insignificant).

Ideal morphological variants proposed for tempering and enriching the microclimate in English courtyard spaces (based on 107 Cambridge samples)				
Microclimatic effect	Thermal-tempering (TT) potential		Thermal-enriching (TE) potential	
Seasons	*summer*	*winter*	*summer*	*winter*
Building strategies				
Increase courtyard size	insig. (except at night) (Muhaisen, 2006)	sig. (at day) (Muhaisen, 2006)	sig. (when CA < 0.2 Ha)	sig.
Increase H/W ratio	sig. (Rivera-Gómez et al., 2019; Johansson & Yahia, 2020; Muhaisen, 2006; Martinelli & Matzarakis, 2017; Jihad & Tahiri, 2016)	sig. (at night)	sig. (when H/W < 0.2)	insig.
Increase shape index	insig.	insig.	sig.	sig.
Increase W/L ratio	sig. (parallel to wind) (Johansson & Yahia, 2020; Muhaisen, 2006)	insig.	sig. (with E-W axis)	sig. (with E-W axis)
Align axis with E-W	insig. (Lau et al., 2015)	sig. (Johansson & Yahia, 2020; Lau et al., 2015)	sig.	sig.
Landscape strategies				
Increase grass coverage	insig. (Taleghani et al., 2014; Taleghani, Tenpierik & Van Den Dobbelsteen, 2012)	insig. (Taleghani et al., 2014, 2012)	sig.	sig.
Increase tree coverage	sig. (Taleghani et al., 2014, 2012)	sig. (Taleghani et al., 2014, 2012)	sig.	sig.

partitions is pending further discriminant analysis of $\boldsymbol{M}(\boldsymbol{UTCI})$ and $\boldsymbol{\delta}(\boldsymbol{UTCI})$ for both methods (see Table 1). It is noteworthy to find that the validity of HAC clustering increases with K, but this does not appear to be the case for K-means. The mean of $\boldsymbol{M}(\boldsymbol{UTCI})$ and $\boldsymbol{\delta}(\boldsymbol{UTCI})$ for seven K-means and HAC clusters are presented in Table 2.

4.4. Case studies

This section illustrates 10 cases from the 107 courtyard samples representing the synergistic and conflicting scenarios based on the discriminant analysis of 7 K-means and HAC clusters (Fig. 8). Appendix C contains the detailed UTCI maps for the selected 10 courtyard cases.

4.4.1. Synergistic scenarios

Km_I, Hac_I, and Hac_IV represent 22%, 23%, and 14% of the courtyard samples, respectively. They feature significant TT and TE potentials at all times (positive synergistic scenarios). The $\boldsymbol{M}(\boldsymbol{UTCI})$ of the Km_I and Hac_IV clusters are lower than the simulation domain in summer ($\boldsymbol{M}$-1.0 °C) and higher in winter ($\boldsymbol{M}$+1.2 °C); the $\boldsymbol{\delta}(\boldsymbol{UTCI})$ remains highest for Km-I ($\boldsymbol{\delta}$+0.29 °C), greater than that for Hac-I ($\boldsymbol{\delta}$+0.16 °C) during summer daytime, while trivial during winter nighttime. The courtyard that achieves the highest TT and TE potentials is the Chapel Court (29) at St Catherine's College, which features a high façade ratio (VAR > 9) and elongated enclosure form (SI = 1.5) with E–W-orientated axis. The second and third synergistic scenarios are the Old Court (30) and Cloister Court (31) at Queens' College (Appendix C, Fig. C.1-a), which feature a compact floorplan and medium façade ratio (SI = 1, 1.6 < VAR < 2.2), while the tree coverage (VC_c_3d > 18%) also contributes to the synergy of significant TT and TE effects.

The number of negative synergistic scenarios (trivial TT or TE potentials) is very low amongst the 107 courtyard samples. Only two negative courtyards are found: the Whittle Laboratory (100, 101) at the West-Cam site (Appendix C, Fig. C.1-b), where the hot-summer-cold-winter situation is more pronounced. The deep patio results in completely shaded conditions all year round.

4.4.2. Conflicting scenarios

Km_III and Hac_II, representing 27% and 20% of the total courtyard samples, feature significant TT but weak TE potential (conflicting scenarios). The $\boldsymbol{M}(\boldsymbol{UTCI})$ curves for both clusters share a similar pattern, with cooler summer daytime ($\boldsymbol{M}$-0.7 °C) and warmer winter nighttime ($\boldsymbol{M}$+0.8 °C). Hac_II has the lowest $\boldsymbol{\delta}(\boldsymbol{UTCI})$ of all courtyard samples ($\boldsymbol{\delta}$-0.41 °C), which is worse than Km_III ($\boldsymbol{\delta}$-0.36 °C). The representative

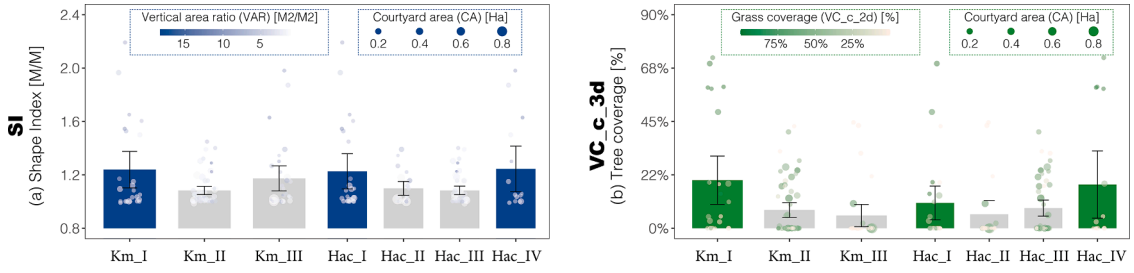

Fig. 9. Summary of morphological differentials from the K-means and HAC clusters: building parameters (a) and landscape parameters (b). Error bars represent ±1.96 standard errors, the 95% confidence interval.

Table A.1-a
6 categories ranked by size to accommodate all 33 simulation domains.

X-Y dimensions (m)	X-Y domain area (Ha)	Boundary offset (m)	Max building height (m)	Number of X-Y grids (3 × 3 m)	Number of domains	Number of courtyards
120 × 120	1.4	24 × 4	30	1600	10	15
150 × 150	2.3	30 × 4	35	2500	7	12
180 × 180	3.2	36 × 4	50	3500	8	27
225 × 225	5.1	45 × 4	45	5625	4	20
270 × 270	7.3	54 × 4	35	8100	1	4
375 × 375	14.1	75 × 4	35	15,625	3	29

Table A.1-b
The assigned materials to the courtyard buildings and landscape in DF.

Buildings	Material name	Material ID	Thickness [m]	Conductivity [$W{\cdot}m^{-1}K^{-1}$]	Specific heat [$J{\cdot}K^{-1}kg^{-1}$]	Albedo [0, 1]	Emissivity [0, 1]
Façade	Brick Wall Reinforced	0100B3	0.3	1.1	840	0.40	0.90
Roof	Roofing Tile	0100R1	0.05	0.84	800	0.50	0.90
Artificial/Natural surface	Concrete pavement grey	0000PG	–	–	–	0.50	0.90
	Asphalt Road	0000ST	–	–	–	0.20	0.90
	Loamy Soil	0100LO	–	–	–	0.00	0.98
	Deep Water	0100WW	–	–	–	0.00	0.96
Landscape	Species/Alternative name	Species ID	Height & diameter [m]	Root depth & width [m]	Transmittance [0, 1]	Foliage albedo [0, 1]	Evaporation [0, 1]
Tree_XL	Quercus Robur (English oak)	0000B3	25 × 15	15 × 25	0.30	0.18	0.7
Tree_L	Platanus & Acerifolia (London/ Hybrid plane)	0000B8	20 × 15	1.5 × 10	0.30	0.18	0.7
Tree_M	Acer Campestre (Field maple)	0000A9	12 × 9	3 × 10	0.30	0.18	0.7
Tree_S	Betula Pendula (Silver birch)	0000B7	6 × 7	1.4 × 10	0.30	0.18	0.7
Grass	Lucerne (Alfalfa)	0100LG	0.18	3	0.30	0.20	0.5

Table A.2-a
The mean of daytime and nighttime roof meteorological data.

Date (day/night)	mT_a [°C]	mRH [%]	mU [$m{\cdot}s^{-1}$]	mU_dir[deg]
17–18-Jul-2021				
05:00 - 20:59	22.91	56.06	3.98	31.84
21:00 - 04:59	19.97	65.41	3.48	195.59
18–19-Jul-2021				
05:00 - 20:59	25.70	51.79	2.92	215.91
21:00 - 04:59	19.97	74.35	3.54	152.94
12–13-Jan-2022				
08:00 - 15:59	1.38	94.27	3.09	280.50
16:00 - 07:59	1.52	93.53	3.60	266.86
13–14-Jan-2022				
08:00 - 15:59	3.61	81.16	3.45	250.55
16:00 - 07:59	0.82	86.37	3.47	259.75

conflicting scenario is Woodlands Court (74) at Girton College, which owns a large area of grassland (CA > 3000 $\mathbf{m}^2$, VC_c_2d > 80%) but is covered by only one English oak tree (VC_c_3d = 12%) (Appendix C, Fig. C.1-c). Comparatively, Cloister Court (73), Ash Court (75), and Campbell Court (76) feature much more compact forms with higher tree coverages (VC_c_3d > 20%) and fall in Km_I and Hac_I clusters (synergistic scenarios).

The rest of the members are pooled into Km_II and Hac_III, which have the largest portions (50% and 43%) of the 107 courtyard samples. They feature weak TT potential but significant TE potential (conflicting scenarios). The $\boldsymbol{\delta}(\boldsymbol{UTCI})$ results of Km-II and Hac-III are slightly greater than that of the simulation domain ($\boldsymbol{\delta}$+0.07 °C). The representatives are 10 courtyards in Churchill College, identical in building envelope but varying in landscape parameters (Appendix C, Fig. C.1-d). Three courtyards with no trees (64, 66, and 71) are clustered into conflicting scenarios which demonstrate homogenous thermal textures. Another three courtyards (65, 68, 69) are the greenest (Vc_c_3d > 50%) showing a significant cooling performance (TT potential) in summer; however, they are not the most thermally diverse because of too much tree coverage. Two other courtyards (66, 68) with less tree coverage (Vc_c_3d = 20%) have the greatest thermal diversities, and the cooling performance is slightly compromised.

5. Discussion

The optimisation of courtyard microclimate is conditional on the flexibility to renew the building enclosure configuration and landscape features. The following discussions will verify the simulation results and emphasise the strengths and limitations of new digital tools to be applied in-situ by design practitioners.

Table A.2-b
The seasonal variation of sun paths at Cambridge.

Hour	Sun_height [Deg]	Sun_azimuth [Deg]	SW_dir_max [$W{\cdot}m^{-2}$]	SW_dir_hor [$W{\cdot}m^{-2}$]	SW_dif [$W{\cdot}m^{-2}$]	Global [$W{\cdot}m^{-2}$]
18-Jul-2021 (BST)						
06:00 (NE sun)	7.2	64.4	222.7	28.0	15.0	43.0
07:00	15.9	75.7	610.9	166.9	51.7	218.6
08:00 (E sun)	24.9	87.0	794.4	334.7	76.6	411.4
09:00	34.1	99.2	896.1	502.1	94.2	596.3
10:00	42.9	113.1	957.0	651.3	106.6	757.9
11:00 (SE sun)	50.7	130.1	993.5	768.9	115.0	883.9
12:00	56.5	151.7	1013.5	845.3	120.0	965.2
13:00 (S sun)	59.0	177.7	1020.4	874.2	121.8	996.0
14:00	57.2	204.1	1015.5	853.5	120.5	974.0
15:00 (SW sun)	51.9	226.5	997.9	784.8	116.1	900.8
16:00	44.3	244.2	964.4	673.4	108.2	781.7
17:00	35.6	258.5	908.4	528.6	96.5	625.1
18:00 (W sun)	26.4	270.9	815.2	363.0	79.9	442.9
19:00	17.3	282.4	649.9	193.5	56.5	250.0
20:00 (NW sun)	8.6	293.6	313.5	46.8	22.2	68.9
13-Jan-2022 (GMT)						
09:00 (SE sun)	5.7	137.1	62.8	6.2	3.9	10.1
10:00	11.1	150.0	399.0	76.9	30.4	107.4
11:00	14.7	163.8	531.9	135.2	44.1	179.3
12:00 (S sun)	16.2	178.2	572.7	159.4	48.8	208.2
13:00	15.3	192.7	548.8	144.8	46.0	190.8
14:00	12.2	206.7	445.0	94.1	34.9	129.0
15:00 (SW sun)	7.2	219.9	187.3	23.4	12.5	35.9

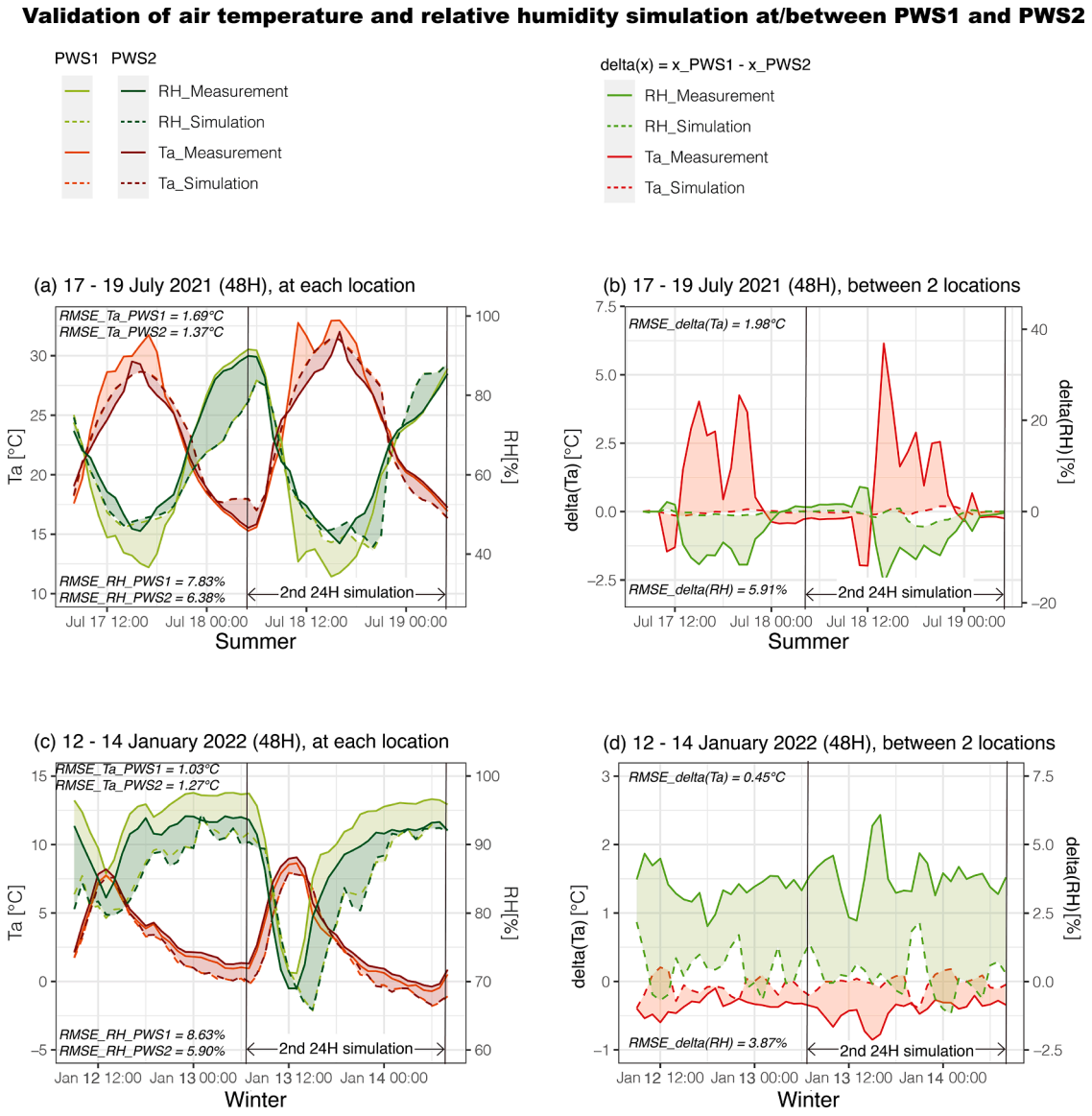

Fig. B.1. The RMSE results of T_a, RH, $delta(T_a)$, and $delta(RH)$ between ENVI-met and 2 PWSs in the courtyard in Churchill College.

5.1. *Verifying the morphological rules of thumb*

We have examined the effective spatial strategies that can have significant microclimatic effect, corresponding to the seven predefined courtyard morphometrics (Table 3). Based on the limited literature on the courtyard microclimate in temperate regions, these morphological rules of thumb are verified with the hybrid-SuperSOM clustering results; for example, the greenest clusters are Km_I, Hac_I, and Hac_IV, which also demonstrate the synergistic TT and TE potentials in the two seasons (Fig. 9).

Generally, landscape approaches are more effective than building approaches in concurrently promoting TT and TE potentials. Such synergistic benefits may result from the evapotranspiration, shading, and photosynthesis of the vegetation, which help to reduce the seasonal thermal extremes and retain the dappled sun-shade texture throughout the year. Another central observation on the green courtyard in promoting nighttime thermal performance extends the previous findings that trees and vegetative grounds can significantly affect outdoor comfort and building energy performance annually (Darvish et al., 2021).

Building parameters require significantly more trade-offs, particularly concerning courtyard size and aspect ratio. Some courtyards with extreme H/W ratio (too deep, too shallow) are presented in Km_III and Hac_II. Though the high walls can effectively offset solar radiation in summer, they also disadvantage solar access in winter; comparatively, these shallow, less enclosed courtyards can invite the winter sun but compromise in shielding against the gusty wind at night, let alone overheating situations in summer (Johansson & Yahia, 2020; River-a-Gómez et al., 2019). Considering the high latitude in Cambridge, winter scenarios should be given more weight to promote the 'sun concentrating character' (Raydan et al., 2004). More than 80% of the 107 courtyard samples are completely shaded at the winter solstice as the highest sun angle is 13.32°; further, the wind conditions can be unpredictable when the trees become defoliated (Konarska et al., 2014).

The building shape index is much higher in the synergistic clusters (I–IV) than in the conflicting ones (II–III). An critical finding is that increasing shape index (non-rectangular enclosure forms) can effectively enrich the courtyard thermal texture, extending the findings of its contribution to indoor daylight reported in previous literature (Taleghani et al., 2012). However, the shape index should be increased with caution because the resultant increase in the façade area has been reported to affect indoor energy use (Quan & Li, 2021; Ratti et al., 2005), though this has not been investigated in this study.

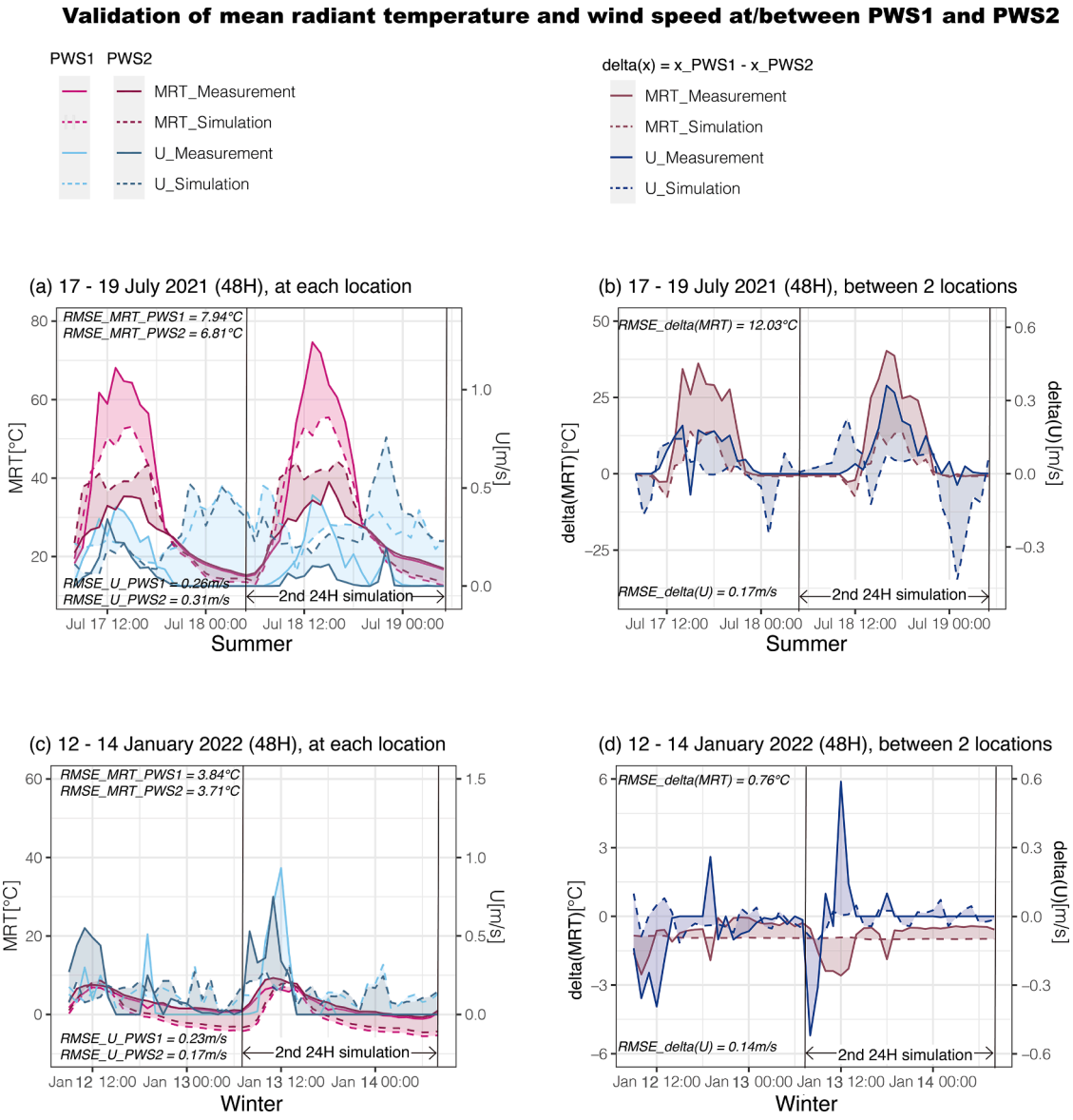

Fig. B.2. The RMSE results of *MRT*, *U*, *delta*(*MRT*), and *delta*(*U*) between ENVI-met and 2 PWSs in the courtyard in Churchill College.

We have found that elongated E–W-orientated courtyards show the more excellent TT and TE potentials (positive synergy) in the two seasons in Cambridge. English courtyards with N–S axes lack sufficient sun due to the building shading from both sides except at noontime, which is conversely considered a cooling advantage in tropical and subtropical regions (Jihad & Tahiri, 2016). Axial strategies are also subject to the HAR (width-to-length ratio), which can affect the depths to which the roof wind reaches. No significant HAR differences have been identified between all hybrid-SuperSOM clusters in this study, which the uncertainty in the wind directions may explain.

5.2. *Designing for non-extreme and enriched thermal experience in historical and new courtyards*

Promotion urban courtyard fabrics, tempering performance, and thermal diversity aligns with the ongoing preservation of vernacular urban and townscapes in Cambridgeshire and worldwide (Cullen, 2012; Edwards et al., 2006; Sunikka-Blank & Galvin, 2016). Our results show that most old courtyards are much more thermally tempered and diverse than those newly built-in West Cambridge. A few exceptions to diverse microclimate include the deep and bare courtyards in central Cambridge, where the sun never reaches the floor. The challenges of microclimate retrofit in those old deep patios also come from the strict planning restrictions in the conservation area. One possible solution is to seek permission for a micro-retrofit of the ground surface, such as adding an extra pervious pavement to reduce the humidity-associated cold stress during winter. Other flexible solutions include the design of miniature landscape elements, such as vertical greenings with an air cavity between the foliage and façade to facilitate the vertical air flow and thus reduce the ground-level humidity. It is essential to bear in mind that the choice of vegetation in a deep courtyard also depends on their lifecycles in a shaded environment (Perini et al., 2013).

Comparatively, there are more opportunities to shape a non-extreme and diverse microclimate through heuristic modelling tools at the early stages of courtyard design. Though many design variants are uncertain at early stages (Wu et al., 2021), static modelling approaches (GH Ladybug, SOLWEIG, Rayman) can allow multiple rounds of geometric testing with relatively low computational cost (Tapias & Schmitt, 2014). The CFD-driven model requires a much longer simulation time than those static, simplified algorithms; however, the results are much more stable and accurate in matching up with the ground-truth data. Therefore, ENVI-met and other compute-heavy programs are not

Fig. C1. UTCI maps of synergistic (225 –∘ 225 m) (a, b) and conflicting scenarios (375 –∘ 375 m) (c, d). Red points and round buffers mark the locations and sizes of tree canopies surrounding the courtyards.

recommended for testing uncertain, early-stage design schemes but are suitable for detailed district plans at later stages, which may include complicated wall materials, vegetation, water bodies, and urban furniture.

5.3. *Limitations and further steps*

This paper has some limitations. For example, simplifying courtyard geometry, building materials, and landscape parameters for modelling make it variable in actual situations. Furthermore, due to lack of geometry data, the semi-outdoor hallways and arcades were removed, which could affect the ventilation at ground level in real-life cases. In addition, identical roof-meteorological parameters were assumed for 33 simulation domains. As a result, the inter-domain air temperature variations were not considered as in real situations. Further improvements could be made by exploring the 'nesting-grid' functions in ENVI-met that allow for varied boundary conditions. We will require better streamlining of the huge computation costs arising from a large single simulation domain. Correspondingly, expanded field measurement at the urban mesoscale is also contingent on the availability of well-calibrated monitors mounted at a number of points of interest for longitudinal validation.

Another limitation regards the exclusion of morphological variables from the machine-learning process, as these variables have the potential to confound or violate the microclimatic-topological structures on Kohonen maps. Further steps can be made by exploring causal-SOM maps based on discrete learnings of the morphometrics and microclimate profiles between courtyards.

6. Conclusions

Real-world courtyards serve as a bridge between simple modelling archetypes and more complex urban-fabric variants. This study attempts to quantify the microclimatic dissimilarities amongst 107 Cambridge courtyards in two seasons. We have identified the significant microclimatic effects of the built and natural forms of courtyards, given the fact that only two cases were identified as negative-synergistic scenarios with trivial thermal-tempering (TT) and thermal-enriching (TE) potentials. The nature-based solutions (vegetative grounds and trees) can promote non-extreme and diverse microclimates more effectively than changing the building parameters. The actual measurement data in Churchill Courtyard has shown good agreement with the ENVI-met model, despite the limitations of using Kestrel 5400 to measure MRT (Appendix B). While there are still many unanswered questions about the optimal courtyard enclosure, the present results are significant in at least four aspects:

(1) The TT potentials in Cambridge courtyards are much smaller than those in hot-arid and tropical climate regions reported in other literature. The average $\boldsymbol{M}(\boldsymbol{UTCI})$ within the English courtyards can be reduced by around 0.6 °C from that of the simulation domains (1.4 to 14 Ha) in summer daytime (5:00 – 21:00 BST) and can be increased by around 1 °C in winter nighttime (16:00 – 8:00 GMT).
(2) A new metric, spatial-UTCI deviation, effectively quantifies the TE potentials within the English courtyards. The average $\boldsymbol{\delta}(\boldsymbol{UTCI})$ is three times higher in summer (+3 °C) than in winter (+1 °C) due to the drastic changes in the sun azimuths and altitudes angles in Cambridge. The dynamic wind directions also contribute to such distinct seasonal profiles.
(3) Courtyards that are deep or bare have similar $\boldsymbol{M}(\boldsymbol{UTCI})$ and $\boldsymbol{\delta}(\boldsymbol{UTCI})$ curves. In contrast, courtyards that are spacious or green are more distinct and diversified in thermal behaviours. Increasing shape index can promote intra-courtyard thermal diversity while its contributions to inter-courtyard thermal diversity is not certain.
(4) The $\boldsymbol{\delta}(\boldsymbol{UTCI})$ curve demonstrate more seasonal and diurnal fluctuations than the $\boldsymbol{M}(\boldsymbol{UTCI})$ curve. Medium-depth courtyard forms ($H/W = 0.5$) with circa 20% deciduous tree coverages have greater synergy between TT and TE potentials in the two seasons. The winter scenarios deserve more attention as the cold northerly weather constitutes a higher annual proportion in oceanic-climate regions. The winter solar access and thermal diversity are higher in elongated courtyards with an E–W axis.

Regarding the implications for practitioners, the preservation and promotion of urban courtyard fabrics in urban regeneration plans and new urban designs can be further justified by microclimate modelling, validation, and testing of heuristic AI tools. Our quantitative findings also identify the challenges posed by humidity-associated cold stress and lack of solar access in the deep and bare courtyards in historical urban contexts. The environmental benefits of micro retrofits, e.g., vertical greening strategies that can enrich the ambient thermal texture and offer visual-thermal delight in the historical courtyards, warrant more attention from policy makers who deal with heritage regulations and legislation that are primarily concerned with aesthetic values. In addition, we show how evidence-based decisions can be made in heritage conservation using a combination of existing micro-climatic simulation toolkits with cutting-edge AI algorithms, which otherwise become resource-intensive and time-consuming with traditional survey-based approaches.

Declaration of Competing Interest

The authors declare that they have no known competing financial interests or personal relationships that could have appeared to influence the work reported in this paper.

Acknowledgments

We would like to take this opportunity to acknowledge the time and effort devoted by the editors and reviewers to improving the quality of this published work. Additionally, ZP would like to thank Mr. Joseph Racosky from Nielsen-Kellerman Ltd and Mr. David Ellis from Richard Paul Russell Ltd for loaning the Kestrel instrument as well as Churchill College for providing a safe environment for the measurement campaigns in 2021 and 2022. RD would like to thank Quadrature Climate Foundation, Laudes Foundation and Churchill College for the support.

Appendix A

Appendix A corresponds to Section 3.2 in Material and Methods. A total of 33 simulation domains (125.8 **Ha**) were sized at six spatial scales (Table A.1-a) to cover the 107 courtyard samples and to optimise the computational cost. The computations were performed on a desktop PC (Dell Precision 5820, quad-core Intel Xeon 4 GHz CPU, 16 GB RAM). All soil types, building façade and roof materials, and river depths were approximated into single categories in DF, due to lack of data from the geo-database and onsite survey (Table A.1-b).

Air temperature ($\boldsymbol{T_a}$), dew point temperature (T_d), relative humidity (*RH*), sunshine hours (*H*), wind speed (*U*), and wind direction (*U_dir* at every 22.5°) are available at 30-min intervals (Table A.2-a). Due to the lack of shortwave and longwave radiation from all RWS databases, the radiation input was generated based on the ENVI-met sun path model. Accordingly, the PWS data on four fully sunny days (17-Jul-2021, 18-Jul-2021, 12-Jan-2022, and 13-Jan-2022) were extracted from the 240-hour observations (Table A.2-b).

Appendix B

Appendix B corresponds to Section 4.1 and shows the validations of simulation results of air temperature and humidity (Fig. B.1), and mean radiant temperature and wind speed (Fig. B.2). Less area of colour shading means more accurate simulation results. In summer, the ENVI-met simulation underestimated the *MRT* in the sun (PWS1) (< 20 °C) and overestimated that under the tree (PWS2) (< 15 °C). In winter, the *MRT*s at both locations were slightly underestimated (< 5 °C), while *delta*(*MRT*) between the two locations was steadier as the courtyard remains shaded throughout the day. *RH* and *U* show higher accuracies in the drier and less windy summer. The simulation accuracies of T_a and *MRT* are generally higher in January than in July. It is worth noting that the validation validity also depends on the calibration statuses of the two PWSs and the degrees of error from the *MRT*

conversion equation based onT_g, T_a, and U data. The small-diameter Kestrel devices can result in 1 to 3 °C error especially when U is high.

Appendix C

Appendix C corresponds to Section 4.4 and shows the intra-courtyard thermal textures of 10 synergistic and conflicting courtyards based on the spatial mean and spatial deviation of daytime and nighttime UTCI in two seasons. Fig. C1. UTCI maps of synergistic (225 × 225 m) (a, b) and conflicting scenarios (375 × 375 m) (c, d). Red points and round buffers mark the locations and sizes of tree canopies surrounding the courtyards.

References

Aune-Lundberg, L., & Strand, G. H. (2014). Comparison of variance estimation methods for use with two-dimensional systematic sampling of land use/land cover data. *Environmental Modelling & Software, 61*, 87–97.

Bardhan, R., et al. (2018). Low-income housing layouts under socio-architectural complexities: A parametric study for sustainable slum rehabilitation. *Sustainable Cities and Society, 41*, 126–138.

Beatley, T. (2011). *Biophilic cities: Integrating nature into urban design and planning*. Island Press.

Berkovic, S., Yezioro, A., & Bitan, A. (2012). Study of thermal comfort in courtyards in a hot arid climate. *Solar Energy, 86*(5), 1173–1186.

Bogaert, J., et al. (2000). Alternative area-perimeter ratios for measurement of 2D shape compactness of habitats. *Applied Mathematics and Computation, 111*(1), 71–85.

Brentan, B., et al. (2018). Hybrid SOM+k-Means clustering to improve planning, operation and management in water distribution systems. *Environmental Modelling & Software, 106*, 77–88.

Chatzipoulka, C., Steemers, K., & Nikolopoulou, M. (2020). Density and coverage values as indicators of thermal diversity in open spaces: Comparative analysis of London and Paris based on sun and wind shadow maps. *Cities, 100*, Article 102645 (London, England).

Chon, T. S., et al. (1996). Patternizing communities by using an artificial neural network. *Ecological Modelling, 90*(1), 69–78.

Chris Mackey, A. D. N., Vasanthakumar, S., Szilasi, A., Song, A., & Roudsari, M. S. (2020). *Ladybug-tools/dragonfly-legacy*. Github.

Costa, J. A. F., & Netto, M. L. D. A. (1999). Estimating the number of clusters in multivariate data by self-organizing maps. *International Journal of Neural Systems, 9*(03), 195–202.

Cullen, G. (2012) Concise Townscape.

Darvish, A., Eghbali, G., & Eghbali, S. R. (2021). Tree-configuration and species effects on the indoor and outdoor thermal condition and energy performance of courtyard buildings. *Urban Climate, 37*, Article 100861.

Del Rio, M. A., et al. (2019). Evaluation of passive cooling methods to improve microclimate for natural ventilation of a house during summer. *Building and Environment, 149*, 275–287.

Diz-Mellado, E., et al. (2021). Extending the adaptive thermal comfort models for courtyards. *Building and Environment, 203*, Article 108094.

Duan, W., et al. (2022). Regional collaboration to simultaneously mitigate PM2.5 and O3 pollution in Beijing-Tianjin-Hebei and the surrounding area: Multi-model synthesis from multiple data sources. *Science of The Total Environment, 820*, Article 153309.

Edwards, B., et al. (2006). *Courtyard housing: Past, present and future*. Taylor & Francis.

Ejarque-Gonzalez, E., & Butturini, A. (2014). Self-organising maps and correlation analysis as a tool to explore patterns in excitation-emission matrix data sets and to discriminate dissolved organic matter fluorescence components. *PloS one, 9*(6), e99618.

Fanger, P. O. (1970). Thermal comfort. Analysis and applications in environmental engineering. Thermal comfort. *Analysis and Applications in Environmental Engineering*.

Forouzandeh, A. (2021). Prediction of surface temperature of building surrounding envelopes using holistic microclimate ENVI-met model. *Sustainable Cities and Society, 70*, Article 102878.

Havenith, G., et al. (2012). The UTCI-clothing model. *International Journal of Biometeorology, 56*(3), 461–470.

Heschong, L. (1979). *Thermal delight in architecture*. MIT press.

Hu, X., & Weng, Q. (2009). Estimating impervious surfaces from medium spatial resolution imagery using the self-organizing map and multi-layer perceptron neural networks. *Remote Sensing of Environment, 113*(10), 2089–2102.

Jacobs, C., et al. (2020). *Are urban water bodies really cooling?, 32*. Urban Climate, Article 100607.

Jendritzky, G., de Dear, R., & Havenith, G. (2012). UTCI–why another thermal index? *International journal of biometeorology, 56*(3), 421–428.

Jihad, A. S., & Tahiri, M. (2016). Modeling the urban geometry influence on outdoor thermal comfort in the case of Moroccan microclimate. *Urban Climate, 16*, 25–42.

Johansson, E., & Yahia, M. W. (2020). Wind comfort and solar access in a coastal development in Malmö, Sweden. *Urban Climate, 33*, Article 100645.

Kohonen, T. (1982). Self-organized formation of topologically correct feature maps. *Biological Cybernetics, 43*(1), 59–69.

Konarska, J., et al. (2014). Transmissivity of solar radiation through crowns of single urban trees—Application for outdoor thermal comfort modelling. *Theoretical and Applied Climatology, 117*(3–4), 363–376.

Lau, K. K. L., et al. (2015). The effect of urban geometry on mean radiant temperature under future climate change: A study of three European cities. *International Journal of Biometeorology, 59*(7), 799–814.

Liu, S., et al. (2021). Dynamic thermal pleasure in outdoor environments - temporal alliesthesia. *Science of The Total Environment, 771*, Article 144910.

López-Cabeza, V. P., et al. (2018). Courtyard microclimate ENVI-met outputs deviation from the experimental data. *Building and Environment, 144*, 129–141. P.

Manioğlu, G., & Oral, G. K. (2015). Effect of courtyard shape factor on heating and cooling energy loads in hot-dry climatic zone. *Energy Procedia, 78*, 2100–2105.

Mänty, J., & Pressman, N. (1988). *Cities designed for winter*. Building Book Limited. Vol. 12.

Martin, L., Martin, L. A., & March, L. (1972). *Urban space and structures*. Cambridge University Press.

Martinelli, L., & Matzarakis, A. (2017). Influence of height/width proportions on the thermal comfort of courtyard typology for Italian climate zones. *Sustainable Cities and Society, 29*, 97–106.

Mcloughlin, F., Duffy, A., & Conlon, M. (2015). A clustering approach to domestic electricity load profile characterisation using smart metering data. *Applied Energy, 141*, 190–199.

Mehrotra, S., Bardhan, R., & Ramamritham, K. (2020). Diurnal thermal diversity in heterogeneous built area: Mumbai, India. *Urban Climate, 32*, Article 100627.

Moonen, P., Dorer, V., & Carmeliet, J. (2011). Evaluation of the ventilation potential of courtyards and urban street canyons using RANS and LES. *Journal of Wind Engineering and Industrial Aerodynamics, 99*(4), 414–423.

Muhaisen, A. S. (2006). Shading simulation of the courtyard form in different climatic regions. *Building and Environment, 41*(12), 1731–1741.

Natanian, J., et al. (2019). Synergetic urban microclimate and energy simulation parametric workflow. In *Proceedings of the journal of physics: conference series*. IOP Publishing.

Natanian, J., & Auer, T. (2020). Beyond nearly zero energy urban design: A holistic microclimatic energy and environmental quality evaluation workflow. *Sustainable Cities and Society, 56*, Article 102094.

Nations, U. (2015) Sustainable development goals–Goal 11: Make cities inclusive, safe, resilient and sustainable.

Nikolopoulou, M. (2011). Outdoor thermal comfort. *Frontiers in Bioscience, 3*(1), 1552–1568.

Nikolopoulou, M., Baker, N., & Steemers, K. (2001). Thermal comfort in outdoor urban spaces: Understanding the human parameter. *Solar Energy, 70*(3), 227–235.

Office, M. (2012). Met office integrated data archive system (MIDAS) land and marine surface stations data (1853-current). *NCAS British Atmospheric Data Centre*.

Park, S., Tuller, S. E., & Jo, M. (2014). Application of Universal Thermal Climate Index (UTCI) for microclimatic analysis in urban thermal environments. *Landscape and Urban Planning, 125*, 146–155.

Parkinson, T., De Dear, R., & Candido, C. (2012). Perception of transient thermal environments: pleasure and alliesthesia. In *Proceedings of the 7th windsor conference*.

Peng, Z., et al. (2022a). Urban climate walk: A stop-and-go assessment of the dynamic thermal sensation and perception in two waterfront districts in Rome, Italy. *Building and Environment*, Article 109267.

Peng, Z., Bardhan, R., & Steemers, K. (2022).The effects of urban morphology on enriching thermal experience: Microclimates of courtyard spaces in Cambridge.

Perini, K., et al. (2013). Vertical greening systems, a process tree for green façades and living walls. *Urban Ecosystems, 16*(2), 265–277.

Perini, K., et al. (2017). Modeling and simulating urban outdoor comfort: Coupling ENVI-Met and TRNSYS by grasshopper. *Energy and Buildings, 152*, 373–384.

Qu, S., et al. (2021). Multiple factors control groundwater chemistry and quality of multi-layer groundwater system in Northwest China coalfield — Using self-organizing maps (SOM). *Journal of Geochemical Exploration, 227*, Article 106795.

Quan, S. J., & Li, C. (2021). Urban form and building energy use: A systematic review of measures, mechanisms, and methodologies. *Renewable and Sustainable Energy Reviews, 139*, Article 110662.

Ratti, C., Baker, N., & Steemers, K. (2005). Energy consumption and urban texture. *Energy and Buildings, 37*(7), 762–776.

Ratti, C., Raydan, D., & Steemers, K. (2003). Building form and environmental performance: Archetypes, analysis and an arid climate. *Energy and Buildings, 35*(1), 49–59.

Raydan, D., Ratti, C., & Steemers, K. (2004). *Courtyards: A bioclimatic form?, in courtyard housing* (pp. 214–229). Taylor & Francis.

Reynolds, J. (2002). *Courtyards: Aesthetic, social, and thermal delight*. John Wiley & Sons.

Rivera-Gómez, C., et al. (2019). Tempering potential-based evaluation of the courtyard microclimate as a combined function of aspect ratio and outdoor temperature. *Sustainable Cities and Society, 51*, Article 101740.

Rodríguez-Algeciras, J., et al. (2018). Influence of aspect ratio and orientation on large courtyard thermal conditions in the historical centre of Camagüey-Cuba. *Renewable energy, 125*, 840–856.

Rojas-Fernández, J., et al. (2017). Correlations between GIS-based urban building densification analysis and climate guidelines for Mediterranean courtyards. *Sustainability, 9*(12), 2255.

Salata, F., et al. (2016). Urban microclimate and outdoor thermal comfort. A proper procedure to fit ENVI-met simulation outputs to experimental data. *Sustainable Cities and Society, 26*, 318–343.

Shanmuganathan, S., Sallis, P., & Buckeridge, J. (2006). Self-organising map methods in integrated modelling of environmental and economic systems. *Environmental Modelling & Software, 21*(9), 1247–1256.
Sheridan, S. C., & Lee, C. C. (2011). The self-organizing map in synoptic climatological research. *Progress in Physical Geography: Earth and Environment, 35*(1), 109–119.
Shirowzhan, S., et al. (2018). Spatial compactness metrics and Constrained Voxel Automata development for analyzing 3D densification and applying to point clouds: A synthetic review. *Automation in Construction, 96*, 236–249.
Soflaei, F., et al. (2017). The impact of courtyard design variants on shading performance in hot-arid climates of Iran. *Energy and Buildings, 143*, 71–83.
Standard, I. (1998). ISO 7726 Ergonomics of the thermal environment-Instruments for measuring physical quantities. *ISO Stand, 1998*, 1–56.
Steemers, K., et al. (1997). City texture and microclimate. *Urban Design Studies, 3*(1997), 25–50.
Steemers, K., & Ramos, M. (2009). Urban environment diversity and human comfort. *Designing High-Density Cities: For Social and Environmental Sustainability*, 107.
Sugg, J. W. (2021). Exploratory geovisualization of the character and distribution of American climate change beliefs. *Weather, Climate, and Society, 13*(1), 67–82.
Sunikka-Blank, M., & Galvin, R. (2016). Irrational homeowners? How aesthetics and heritage values influence thermal retrofit decisions in the United Kingdom. *Energy Research & Social Science, 11*, 97–108.
Taleghani, M., et al. (2014a). Heat mitigation strategies in winter and summer: Field measurements in temperate climates. *Building and Environment, 81*, 309–319.
Taleghani, M., Tenpierik, M., & Van Den Dobbelsteen, A. (2012). Environmental impact of courtyards—A review and comparison of residential courtyard buildings in different climates. *Journal of Green Building, 7*(2), 113–136.
Taleghani, M., Tenpierik, M., & van den Dobbelsteen, A. (2014b). Indoor thermal comfort in urban courtyard block dwellings in the Netherlands. *Building and Environment, 82*, 566–579.
Tapias, E., & Schmitt, G. (2014). Climate-sensitive urban growth: Outdoor thermal comfort as an indicator for the design of urban spaces. *WIT Transactions on Ecology and the Environment, 191*, 623–634.
Tian, J., Azarian, M. H., & Pecht, M. (2014). Anomaly detection using self-organizing maps-based k-nearest neighbor algorithm. In *Proceedings of the PHM society European conference*.
Wehrens, R., & Buydens, L. M. (2007). Self-and super-organizing maps in R: The Kohonen package. *Journal of Statistical Software, 21*, 1–19.
Wu, Y., et al. (2021). A surrogate-assisted optimization framework for microclimate-sensitive urban design practice. *Building and Environment, 195*, Article 107661.
Yaşa, E., & Ok, V. (2014). Evaluation of the effects of courtyard building shapes on solar heat gains and energy efficiency according to different climatic regions. *Energy and Buildings, 73*, 192–199.
Zamani, Z., Heidari, S., & Hanachi, P. (2018). Reviewing the thermal and microclimatic function of courtyards. *Renewable and Sustainable Energy Reviews, 93*, 580–595.